CAPACITY AND DRIVEABILITY OF 50 KSI H-PILES

by

Marwa Hasanzoi

Bachelor of Science, Kabul University, 2011

Submitted to the Graduate Faculty of

Swanson School of Engineering in partial fulfillment

of the requirements for the degree of

Master of Science

University of Pittsburgh

2015

UNIVERSITY OF PITTSBURGH

SWANSON SCHOOL OF ENGINEERING

This thesis was presented

by

Marwa Hasanzoi

It was defended on

March 23rd, 2015

and approved by

Kent A. Harries, Ph.D., Associate Professor

Jeen-Shang Lin, Ph.D., Associate Professor

John C Brigham, Ph.D., Assistant Professor

Thesis Advisor: Kent A. Harries, Ph.D., Associate Professor

CAPACITY AND DRIVEABILITY ASSESSMENT OF 50 KSI H-PILES

Marwa Hasanzoi, M.S.

University of Pittsburgh, 2015

H-piles are widely used to support bridge piers and foundations, particularly those founded on relatively weak subsoil layers. The piles are forcefully driven to stronger layers to transfer the load of the entire structure to the bearing strata. Driven steel H-piles are designed to effectively interact with their surrounding environment in and out of the ground without failure. Standard practices such as AASHTO/LRFD and state codes regulate the load bearing capacity and drivability of H-piles to ensure safe performance during their service life.

This thesis investigates the feasibility of installing H-piles considering the limitations on the driving stress to achieve the design capacity ($\alpha A_S F_y$). Effects of parameters related to the soil-pile-hammer system have been studied. The gradual development of standard practices regulating the properties of H-piles related to material type, cross section geometry, pile length, and driving stress is discussed focusing on AASHTO/LRFD and PennDOT revisions to AASHTO. The results of a comprehensive parametric study carried out on the soil-pile-hammer system for 50 ksi driven H-piles are presented. 126 base scenarios, and 15 sensitivity analyses were constructed and analyzed using computer program GRLWEAP. In addition, 11 benchmark scenarios were considered to validate the study methodology approach using field data provided by PennDOT. An additional application of H-piles as driven ‘extended piles’ under combined axial and lateral load is briefly discussed and the effects of soil-pile interaction on the performance of pile is investigated.

TABLE OF CONTENTS

1.0 INTRODUCTION AND LITERATURE REVIEW 1

1.1 INTRODUCTION 1

1.2 ISSUES ASSOCIATED WITH ADOPTION OF F_Y = 50 KSI FOR H-PILE DESIGN 4

1.2.1 Structural steel capacity 4

1.2.2 Effect of corrosion 6

1.2.3 Allowable net settlement limit 7

1.2.4 Tip bearing capacity 8

1.2.5 Driving stresses and the need for a driving Tip 8

1.2.6 Friction describes as "Shaft Percentage" 9

1.3 H-PILE STRUCTURAL DESIGN CRITERIA 9

1.3.1 Material resistance factors 9

1.3.2 PennDOT application of resistance factors 11

1.3.3 Compressive resistance of piles 12

1.3.4 Weak axis flexural resistance of H-piles 14

1.3.5 Strong axis flexural resistance of H-piles..... 15

1.3.6 Reduced cross sections due to assumed effect of corrosion..... 15

1.3.7 Capacity of standard HP sections..... 16

1.4 PENNDOT EXPERIENCE AND PRACTICE 18

1.4.1 I-95/I-276 Interchange pile testing program (PTC 2011)..... 23

1.5 GEOTECHNICAL RESISTANCE OF DRIVEN PILES..... 25

1.5.1 AASHTO LRFD/DM-4 §10.7.3.8.6 – Pile bearing resistance 26

1.5.2 Static analysis methods for determining nominal bearing resistance of piles in cohesionless soils 26

1.5.3 Static analysis methods for determining nominal bearing resistance of piles in cohesive soils..... 27

1.5.4 Nominal bearing capacity of piles on rock 28

1.5.5 Minimum pile penetration 31

1.6 DYNAMIC ANALYSIS OF PILES (WEAP)..... 32

2.0 PARAMETRIC STUDY METHODS AND MATRIX..... 35

2.1 METHODOLOGY 36

2.2 PARAMETER SELECTION 38

2.2.1 Pile section 38

2.2.2 Hammer types, weights and cushions 39

2.2.3 Soil types above rock 39

2.2.4 Shaft friction 40

2.2.5 Pile length 40

2.2.6 Benchmark scenarios 41

3.0 RESULTS OF PARAMETRIC STUDY AND DISCUSSION 43

3.1 OBSERVATIONS FROM WEAP ANALYSES 45

3.1.1 Driving stress 45

3.1.2 Pile ultimate capacity 47

3.1.3 Range of hammer stroke 48

3.1.4 Varying driving parameters 49

3.1.5 Ratio of driving stress to ultimate stress 51

3.1.6 Conclusions based on present code provisions 52

3.1.7 Benchmark scenarios: GRLWEAP analyses results 53

4.0 EXTENDED STEEL H-PILES 55

4.1.1 Background 55

4.1.2 Analysis methods 56

4.1.3 Effective length (L_e) 58

4.1.4 Pile-to-pile cap connection fixity..... 63

4.1.5 Failure modes of pile under lateral loads 64

4.1.6 Summary..... 66

5.0 CONCLUSIONS 67

APPENDIX A 69

BIBLIOGRAPHY 75

LIST OF TABLES

Table 1 Historical basic allowable stresses (ksi) in AISC specifications (Brockenbrough 2002).. 2

Table 2 AASHTO LRFD and PennDOT DM-4 section slenderness limits. 5

Table 3 Gross section slenderness and the impact 1/16 in. section loss on flange slenderness..... 6

Table 4 Material resistance factors for steel H-piles. 10

Table 5 Effective material resistance factors for axial load..... 12

Table 6 Impact of increasing Fy from 36 ksi to 50 ksi and prescribed 1/16 in. section reduction on axial and flexural capacities of HP sections. 17

Table 7 GRLWEAP input variables used by PennDOT. 19

Table 8 Maximum compressive stress determined in field and predicted by GRLWEAP for five example cases (Forscht 2012). 20

Table 9 Summary of H-pile capacity in weak shale (Watral 2013). 21

Table 10 Pile test details and results from PTC Pile Test Program (PTC 2011). 24

Table 11 Resistance factors for single driven piles, ϕ_{stat} (DM-4 Table 10.5.5.2.3-1). 26

Table 12 Summary of static analysis methods for piles in cohesionless soils 30

Table 13 Summary of static analysis methods for piles in cohesive soils. 31

Table 14 Recommended quake values for impact driven piles (PDI 2010). 34

Table 15 Recommended damping values for impact driven piles (PDA, 2010). 34

Table 16 Hammer parameters used in this study 39

Table 17 Analysis parameter matrix 40

Table 18 Results of WEAP analysis for HP12x74 43

Table 19 Ratio of driving stress over ultimate stress 52

Table 20 Benchmark scenarios analyses results 54

Table 21 Rate of increase of soil modulus with depth n_h (ksi/ft) for sand 59

LIST OF FIGURES

Figure 1 Conceptual representation of WEAP analysis. 32

Figure 2 Driving stress distribution 47

Figure 3 Pile ultimate capacity 48

Figure 4 Hammer stroke available 49

Figure 5 Pile ultimate capacity 50

Figure 6 Driving stress 51

Figure 7 Examples of HP sections pile bents 55

Figure 8 Equivalent model of fixed-head pile by Wilson et al. 1963. 59

Figure 9 Equivalent elastic model by Robinson et al. 2006. 61

Figure 10 Equivalent model for a fixed-head extended pile by Shama et al. 2002. 63

Figure 11 Failure modes for (a) free-head & (b) fixed-head boundary conditions (Fatahi et al., 2014) 65

1.0 INTRODUCTION AND LITERATURE REVIEW

1.1 INTRODUCTION

Driven pile foundations are a type of deep foundation or pile foundation, where the structure is supported on deeper and stronger geologic materials in the case of weaker subsurface ground materials. Pile foundations can carry a large amount of axial load while occupying a relatively small area. They are also capable of resisting a large amount of uplift and lateral load. Structural steel and prestressed concrete are the most common types of driven piles. Steel H-piles find common application in short and medium span bridge foundations in North America. Driven steel H-piles are cost-effective, more ductile and flexible than concrete alternatives and can easily penetrate into soft bedrock, reaching firm strata to establish end-bearing capacity. Driven H-piles provide higher end-bearing resistance with low side resistance.

The application of hot-rolled structural steel shapes goes back to 1880s, when steel replaced cast iron and wrought iron that were the most common construction materials at that time (Brockenbrough, 2003). This also marks the start of the application of steel piles in deep foundations. Considering only axial compressive capacity of fully-braced (i.e., $l/r = 0$) sections, the allowable stress for sections remained essentially unchanged from the 1920's to the 1960's at 17 ksi. During this time, the specified yield capacity of ASTM A9 steel increased incrementally to 36 ksi. In 1961 major revisions were made to ASD standards introducing ASTM A36 material

specification for carbon structural steel having a typical yield value F_y = 36 ksi. In 1963 ASD introduced minimum yield stress (F_y) requirements and defined allowable stresses in terms of F_y. In 1969 additional revision were made permitting ASTM A572 for high-strength low-alloy structural steel and the minimum yield stress range was extended to 100 ksi although the typical value of yield for ASTM A572 was F_y = 50 ksi. Table 1 shows the historic evolution of allowable stress for fully braced steel compression members since 1923.

Table 1 Historical basic allowable stresses (ksi) in AISC specifications (Brockenbrough 2002).

AISC Specification	**Typical expected yield strength of H-piles (ASCE 41-13 Table 9-1)**	**Compression (*l/r* = 0)**
1923	ASTM A9: 28 ksi	18 ksi
1936	ASTM A9: 33 ksi	17 ksi
1963-1989	ASTM A36: 36 – 44 ksi ASTM A572: 50 ksi	$0.60F_y$
1990-present	ASTM A572: 50 ksi	$0.658F_y$

In the present *AISC Steel Construction Manual* (2012), dimensions and property information of twenty-one HP section are given in Table 1-4. The shapes are designated with the HP mark, the nominal depth in inches (d) and the nominal weight in lb/ft. The nominal depth for HP sections ranges from 18 to 8 inches. The sections being investigated in this thesis are those most commonly used by the PennDOT (see Table 3). HP shapes are wide flanged shapes distinguished as having nominal flange widths (b_f) equal to nominal depth (d) and having equal flange (t_f) and web (t_w) thickness. Today, HP shapes are most commonly available in ASTM A572 Grade 50; thus they have a nominal yield strength of F_y = 50 ksi and tensile strength of 65 ksi. However, until fairly recently, HP shapes were typically available as ASTM Grade 36 shapes.

When load and resistance factor design method (LRFD) was established in 1986, providing an alternative to ASD specifications, limit states were introduced in order to ensure functionality and stability of the structural elements under self- and service-loads and sufficient strength under probable design loads and some extreme events. Limit states are intended to limit stresses and deformations of structures under loading demands in order to meet the design requirements during its design life. AASHTO LRFD (2010) §10.7 establishes three limit states for driven piles: service limit state, strength limit state and extreme events with the requirement that strength limit state considerations should satisfy pile design criteria before examining service limit state considerations. A driven H-pile foundation consists of soil-pile system where the two important limit states to be considered is structural limit state (Section 1.3) and geotechnical limit state (Section 1.5). It is noted that under strength limit state the lateral resistance of a driven end-bearing H-pile is purely structural since the soil will not fail under lateral loading rather it will continuously displace with almost constant resistance (AASHTO 2010).

PennDOT Design Manual DM-4 (2012) §6.15.1 limits the specified yield strength of steel piles to $F_y \leq 36$ ksi. PennDOT Strike-Off Letter (SOL) 483-13-12 modifies this limit to $F_y \leq$ 50 ksi and updates relevant sections of DM-4, BC-757M and Publication 408 (section 1005) accordingly. SOL 483-13-12 notes “there is no apparent detrimental effect to bridges supported by H-pile foundations” resulting from this change. Subsequently, SOL 483-14-04 was issued to clarify the current pile design methodology for computing design capacity for H-piles and implements a new design methodology for computing the design capacity of steel pipe piles. This latest SOL revises DM-4 and replaces certain pages of SOL 483-13-12 which implemented the use of $F_y = 50$ ksi for steel H-piles for computing the design capacity.

It is within the present context of LRFD design and commercially available HP-section that this study is made. The primary motivation for making the change from F_y = 36 ksi to F_y = 50 ksi is that the 'preferred material specification' (AISC 2011) for H-pile shapes is ASTM A572 (2013) Grade 50 High Strength-Low Alloy Steel. Even if ASTM A36 (2012) steel were specified (availability may be limited and therefore such specification would be at an increased cost), there is no upper limit on yield strength. Steel fabrication depends on scrap steel, which includes strength-enhancing elements that are not easily removed; therefore it is difficult for manufacturers to produce structural steel with a yield stress below 50 ksi.

An additional motivation is the expected cost savings, resulting from potentially using smaller sections that may be realized by increasing the design capacity. The following section addresses effects and potential risks associated with the increase in design capacity from F_y = 36 ksi to F_y = 50 ksi.

1.2 ISSUES ASSOCIATED WITH ADOPTION OF F_y = 50 KSI FOR H-PILE DESIGN

The following issues have been identified as being potentially impacted by increasing the design strength of H-piles from F_y = 36 ksi to F_y = 50 ksi.

1.2.1 Structural steel capacity

Although the higher yield strength improves stability and yield checks, the higher yield strength may adversely affect ductility checks associated with non-compact shapes. As the yield strength

increases from 36 to 50 ksi, the flange and web slenderness ratios defining compact and noncompact section limits – both a function of $\sqrt{E/F_y}$ – fall 18% (Table 2).

Table 2 AASHTO LRFD and PennDOT DM-4 section slenderness limits.

Design action	**AASHTO/DM-4**	**Plate element**	**Slenderness limit**		
			Calculation	**36 ksi**	**50 ksi**
Axial capacity	§6.9.4.2	Flanges	$b_f/2t_f \le 0.56\sqrt{E/F_y}$	15.9	13.5
		Web	$(d-2k)/t_w \le 1.49\sqrt{E/F_y}$	42.3	35.9
Strong and weak axis flexure	§A6.3.2 (strong) §6.12.2.2.1(weak)	Compact flange	$b_f/2t_f \le 0.38\sqrt{E/F_y}$	10.8	9.2
		noncompact flange	$b_f/2t_f \le 0.83\sqrt{E/F_y}$	23.6	20.0

Of the nine HP shapes typically used by PennDOT (those reported in DM-4 Table 6.15.3.2P and reported here in Table 3), 14x73 and 12x53 become ‘slender for axial load’ when F_y is increased from 36 ksi to 50 ksi. In terms of strong-axis flexure, seven of the nine sections are ‘non-compact for flexure’ at F_y = 50 ksi while only four shapes are non-compact at F_y = 36 ksi. Only 12x84 and 10x57 are compact for both axial and flexural loads for both F_y = 36 ksi and F_y = 50 ksi (see Table 3).

Table 3 Gross section slenderness and the impact 1/16 in. section loss on flange slenderness.

HP	Gross section properties					Reduced section properties				
	$b_f/2t_f$	Axial		Flexure		$b_f/2t_f$	Axial		Flexure	
		36 ksi	50 ksi	36 ksi	50 ksi		36 ksi	50 ksi	36ksi	50ksi
14x117	9.25	Compact	Compact	Compact	***Noncompact***	10.85	Compact	Compact	All are **noncompact**	All are **noncompact**
14x102	10.49	Compact	Compact	Compact	***Noncompact***	12.64	Compact	Compact		
14x89	11.95	Compact	Compact	***Noncompact***	***Noncompact***	14.87	Compact	***Slender***		
14x73	14.44	Compact	***Slender***	***Noncompact***	***Noncompact***	19.03	***Slender***	***Slender***		
12x84	8.97	Compact	Compact	Compact	Compact	10.87	Compact	Compact		
12x74	10.01	Compact	Compact	Compact	***Noncompact***	12.46	Compact	Compact		
12x63	11.77	Compact	Compact	***Noncompact***	***Noncompact***	15.38	Compact	***Slender***		
12x53	13.84	Compact	***Slender***	***Noncompact***	***Noncompact***	19.23	***Slender***	***Slender***		
10x57	9.05	Compact	Compact	Compact	Compact	11.48	Compact	Compact		

It is worth commenting here that the slender and non-compact shapes are ‘barely’ so. While the slender and non-compact designations trigger more robust calculation of capacity, the actual decrease in capacity over the compact shape calculations is at worst 3.6% for axial and 8% for flexural loads (both for the most slender 14x73 shape).

1.2.2 Effect of corrosion

Corrosion resistance of steel piles is unaffected by strength. The use of higher strength piles may permit smaller pile sections to be used to resist the same load. When considering the effects of corrosion, it is typical to assume section loss of 1/16 in. from all surfaces. Thus a pile having a smaller section area has less ‘reserve’ capacity; that is: the 1/16in. reduction in plate thickness represents a proportionally greater section area for a smaller pile. Additionally, as shown in Table 3, the effect of section loss increases the slenderness of the sections. In this case, HP 14x73 and HP 12x53 become slender for axial load when section loss is considered (Table 3).

1.2.3 Allowable net settlement limit

DM-4 §D10.5.2.2 limits net foundation settlement to 1 inch at service loads. For a bearing pile, this net settlement is the sum of two components: Δ_{tip}, tip displacement and Δ_s, pile shortening. Tip displacement is a function of the bearing rock strata modulus and is independent of the pile steel grade. Pile shortening (Δ_s) is given by the relationship:

$$\Delta_s = (Q_p + \zeta Q_s)L/EA \qquad (1)$$

Where Q_p and Q_s are the loads carried by the pile point and the skin friction, respectively; ζ represents the effect of the friction distribution pattern; L is the length of the pile; A the pile cross-section area; and E is the modulus of elasticity of the pile (E_{steel} = 29000 ksi). The load carried by the pile, P, is marginally less than the sum $Q_p + \zeta Q_s$; for simplicity, however, P is used in the following discussion.

While this relationship is independent of steel grade, the pile yield capacity is affected by steel grade. If pile capacity is increased from 36 ksi to 50 ksi, two implications for design may occur: a) the pile capacity, P, increases for the same pile section; or, b) the pile area, A may be reduced to carry the same value of P. Both cases result in an increase in Δ_s. Assuming a perfectly efficient design (i.e.: 100% utilization of cross section A to resist load P), the increase in Δ_s is equal to the ratio 50/36 = 1.39. Increasing Δ_s, while respecting the same net settlement limit, reduces the allowable tip displacement by a corresponding value. For case a) in which the pile capacity is increased, it must be assumed that Δ_{tip} will also increase at least in proportion to the applied load, P. In this case, the net settlement will increase 39% in going from F_y = 36 ksi to F_y = 50 ksi. For case b) the net settlement increase will approach 39% as the ratio Δ_{tip}/Δ_s approaches zero.

Related to this, DM-4 §C10.7.3.8.1 cites the findings of Kulhawy et al. (1983) in reporting that a pile driven in soil must displace on the order of 8% of its diameter in order to fully mobilize the tip capacity. Taking this guidance at face value and limiting settlement to 1 in. means that piles having a diameter greater than 12.5 in. cannot fully mobilize their tip capacity without exceeding settlement limits. This hypothetical calculation additionally neglects the effect of pile shortening. Curiously, Kulhawy et al. is not the source of the 8% value; Kulhawy et al. cites Vesic (1977) in this case. It is not entirely clear the basis for the '8% rule-of-thumb' since this value will be affected by soil type and pile length to a degree.

1.2.4 Tip bearing capacity

While the pile bearing capacity increases as F_y increases from 36 to 50 ksi, the soil into which the pile is driven and the strata on which it bears is unchanged. Thus it is conceivable that a pile system whose limit state is governed by structural capacity at F_y = 36 ksi is governed by geotechnical bearing capacity at F_y = 50 ksi. This may be particularly the case for "weak rock" conditions. A similar argument may be made for the pile cap. A higher strength concrete may be required to satisfy allowable stress limits in the cap as F_y is increased from 36 to 50 ksi.

1.2.5 Driving stresses and the need for a driving Tip

Related to tip bearing capacity, it is equally conceivable that in order to efficiently drive a pile at F_y = 50 ksi, a driving tip is required which may not have been the case for F_y = 36 ksi. The use of the driving tip lowers the capacity of the pile (ϕ decrease from 0.6 to 0.5 (AASHTO) or from 0.45 to 0.35 (DM-4)), reducing the increased pile capacity that may be realised using the higher

strength steel. DM-4 §D10.7.8.5, however, specifically requires driving tips for all point bearing and end bearing piles driven into bedrock.

1.2.6 Friction describes as "Shaft Percentage"

As will be discussed 'shaft percentage' – the portion of bearing pile capacity resisted by friction – is a necessary parameter used in design. The increase in pile strength has no effect on properties affecting friction.

1.3 H-PILE STRUCTURAL DESIGN CRITERIA

The following documents the calculations of axial, strong-axis and weak-axis flexural capacities, P_r, M_{rx} and M_{ry}, respectively. All HP section data is that reported in *AISC Steel Construction Manual* (2012). In this discussion gross section properties are assumed. PennDOT additionally considers pile capacity for deteriorated piles having '1/16 inch section loss' (Table 3). In the latter case, reduced section properties are used in the design equations. Such reduction due to corrosion is discussed in Section 1.3.6.

1.3.1 Material resistance factors

The material resistance factors (ϕ) used for the calculation of steel H-pile capacity are provided in ASHTO LRFD §6.5.4.2 and are summarized in Table 4.

Different ϕ-values are used for axial resistance than for axial when combined with flexure. This is because the lower values are applied only to sections of the pile "likely to experience damage"; these will not be in regions (along the pile length) were combined loads are critical. The material resistance factors for piles are based on recommendations of Davisson et al. (1983) with modifications to reflect current design philosophy (AASHTO LRFD 2010).

Table 4 Material resistance factors for steel H-piles.

<table>
<tr><th></th><th>AASHTO (2010)</th><th>DM-4 (2012)</th><th>SOL 483-13-12 (2013)</th><th>SOL 483-14-04 (2014) Table 6.15.2-1</th></tr>
<tr><td rowspan="2">For axial resistance of piles in compression and subject to damage due to severe driving conditions where use of a pile tip is necessary</td><td rowspan="2">$\phi_c = 0.50$</td><td colspan="2">$\phi_c = 0.35$</td><td>$\phi_c = 0.50$ with $P_n = 0.66A_sF_y$</td></tr>
<tr><td colspan="3">DM-4 §D10.7.8.5 requires driving tips for all point bearing and end bearing piles driven into bedrock</td></tr>
<tr><td>For axial resistance of piles in compression under good driving conditions where use of a pile tip is not necessary</td><td>$\phi_c = 0.60$</td><td colspan="2">$\phi_c = 0.45$</td><td>$\phi_c = 0.60$ with $P_n = 0.66A_sF_y$</td></tr>
<tr><td>For combined axial and flexural resistance of undamaged piles – axial resistance</td><td>$\phi_c = 0.70$</td><td colspan="2">$\phi_c = 0.60$</td><td>$\phi_c = 0.70$ with $P_n = 0.66A_sF_y$</td></tr>
<tr><td>For combined axial and flexural resistance of undamaged piles – flexural resistance</td><td>$\phi_f = 1.00$</td><td colspan="2">$\phi_f = 0.85$</td><td>$\phi_c = 1.00$ with $P_n = 0.66A_sF_y$</td></tr>
<tr><td>For resistance during pile driving</td><td>$\phi = 1.00$</td><td colspan="3">$\phi = 1.00$</td></tr>
<tr><td>For piles bearing on soluble bedrock (limestone, etc.), to provide pile group redundancy and limit the design stress to 9 ksi</td><td>Not considered in §6.5.4.2</td><td>$\phi_c = 0.25$</td><td>$\phi_c = 0.273$</td><td>$\phi_c = 0.273$ with $P_n = 0.66A_sF_y$</td></tr>
<tr><td>§10.7.8 Driveability Analysis</td><td>0.90</td><td>1.00 (36 ksi)
0.80 (50 ksi)</td><td>0.90</td><td>$\phi_c = 0.90$</td></tr>
</table>

1.3.2 PennDOT application of resistance factors

The lower material resistance factors used by PennDOT are reported to be calibrated with load factors to result in the same "factor of safety previously used by the Department" (DM-4 C6.15.2). Beyond this, the justification for lowering the factors beyond those prescribed by AASHTO is unclear since the AASHTO-prescribed factors already reportedly account for all "additional factors" identified as affecting pile capacity. The only interpretation available is that these "additional factors" are more significant in Pennsylvania practice. The result is that the reliability associated with PennDOT practice is unknown although it is greater than that used in AASHTO. Additionally, and potentially of greater concern, the resulting reliability is different for each design case since the ratio of prescribed resistance factors differs (Table 5, column 3).

Anecdotally, PennDOT appears to prescribe and use λ = 1.0 in §6.9.4.1 (Section 1.3.3). However, DM-4 does not modify AASHTO §10.7.3.13.1 which prescribes λ = 0; thus the basis for the $0.66A_sF_y$ calculation (that is λ = 1.0) is uncertain in the context of DM-4. SOL 483-14-04 sheds some light on this issue but does not entirely correct it. In SOL 483-14-04, Table 6.15.2-1 clearly prescribes the AASHTO (2010) resistance factors to be applied to be a nominal axial capacity of $0.66A_sF_y$. This results in effective reduction factors lower than the previously prescribed DM-4 values (see Table 5, column 5) and 66% of those prescribed by AASHTO. (column 6). Without having the explicit statistical variation associated with both material resistance and applied loads, the exact reliability may not be calculated. The concern with the 'dual factor' approach taken by PennDOT is that it masks statistically anticipated behavior, promulgates mechanically incorrect design equations and results in misleading measures of reliability. Nonetheless, current PennDOT practice remains conservative and represents no safety

concerns. The corollary of this is that the resulting pile designs may be unnecessarily uneconomical.

Table 5 Effective material resistance factors for axial load.

1	2	3	4	5	6
AASHTO (2010)	**DM-4 (2012)**	**DM-4 / AASHTO**	**SOL 483-14-04**	**SOL 483-14-04 / DM-4**	**SOL 483-14-04 / AASHTO**
$0.50A_sF_y$	$0.35A_sF_y$	0.70	$0.50(0.66)A_sF_y = 0.33A_sF_y$	0.94	0.66
$0.60A_sF_y$	$0.45A_sF_y$	0.75	$0.60(0.66)A_sF_y = 0.40A_sF_y$	0.89	0.66
$1.0A_sF_y$	$0.85A_sF_y$	0.85	$1.0(0.66)A_sF_y = 0.66A_sF_y$	0.77	0.66

For piles bearing on soluable bedrock (Table 4), the reported intent of DM-4 is to limit the bearing stress to 9 ksi. The material resistance factor is calibrated so that this is the case.

1.3.3 Compressive resistance of piles

AASHTO LRFD/DM-4 §6.15.3 refer to §6.9.2.1 for calculation of P_n as follows:

1. Section geometry is checked against compact plate buckling criteria given by Eq. 6.9.4.2-1:

		36 ksi	**50 ksi**
Flanges	$b_f/2t_f \le 0.56\sqrt{E/F_y}$	15.9	13.5
Web	$(d-2k)/t_w \le 1.49\sqrt{E/F_y}$	42.3	35.9

For HP sections web slenderness is not a concern. The most slender gross section web is an HP 14x73 having a web slenderness of 22.2 while the most slender reduced section web is an HP 12x53 having a slenderness of 30.7.

2. Calculate Axial Capacity per §6.9.4.1.

Although the notation changed from 2007 to 2010, the AASHTO-prescribed calculation of axial capacity is effectively the same: "[the equations given] are equivalent to the equations given in AISC (2005) [and all subsequent editions] for computing the nominal compressive resistance. The equations are written in a different format…" (AASHTO LRFD §C6.9.4.1.1). However, the change in terminology from the λ factor to the capacity ratio P_e/P_o ***appears*** to affect the calculated results for fully-supported piles. However, in both AASHTO LRFD 2007 and 2010, §10.7.3.13.1 states that for fully supported piles, λ = 0. The ratio P_o/P_e can be shown to be mathematically equivalent to λ; therefore, the interpretation of §6.9.4.1 should remain consistent. That is, $P_o/P_e = \lambda$. The change from a factor 0.66 to 0.658 aligns the AASHTO equation with that of AISC (see Table 1) and has a negligible effect (0.3%).

Flange slenderness (see step 1)	**AASHTO LRFD (2007)**	**AASHTO LRFD (2010)**
	$\lambda = \left(\frac{K\ell}{r\pi}\right)^2 \frac{F_y}{E}$ For fully supported piles, λ = 0 (§10.7.3.13.1)	$P_o = QF_yA_s$ and $P_e = \frac{\pi^2 E}{(K\ell/r)^2} A_s$ $P_o/P_e = \lambda$ For fully supported piles, λ = 0 (§10.7.3.13.1)
Compact	$P_n = 0.66^{\lambda} F_yA_s = F_yA_s$	$P_n = 0.658^{Po/Pe} F_yA_s = F_yA_s$
Slender	Member is designed according to AISC as follows (C6.9.4.1): For $0.56\sqrt{E/F_y} \le b_f/2t_f \le 1.03\sqrt{E/F_y}$ $Q_s = 1.415 - 0.74\left(b_f/2t_f\right)\sqrt{F_y/E}$ $P_n = Q_sF_yA_s$	AASHTO LRFD §6.9.4.2.2: For $0.56\sqrt{E/F_y} \le b_f/2t_f \le 1.03\sqrt{E/F_y}$ $Q_s = 1.415 - 0.74\left(b_f/2t_f\right)\sqrt{F_y/E}$ $P_n = Q_sF_yA_s$

PennDOT SOL 483-14-04 Table 6.15.2-1 sets $P_n = 0.66F_yA_s$ and $Q_s = 1.0$ regardless of slenderness. This is a conservative approach since calculated values of Q_s for conventionally

used pile sections (Table 3) do not fall below 0.82 (HP 12x53 having F_y = 50 ksi and 1/16 section loss) in any case.

1.3.4 Weak axis flexural resistance of H-piles

AASHTO LRFD/DM-4 §6.12.2.2.1 calculates weak axis flexural resistance, M_{ny} as follows:

Flange slenderness				M_{ny}
		36 ksi	50 ksi	
Compact flange	$b_f/2t_f \le 0.38\sqrt{E/F_y}$	10.8	9.2	$M_{ny} = M_{py} = 1.5S_yF_y$ (per C6.12.2.2.1)
Noncompact flange	$b_f/2t_f \le 0.83\sqrt{E/F_y}$	23.6	20.0	From AASHTO LRFD Eq. 6.12.2.2.1-2: $M_n = Z_yF_y\left[1-\left(1-\frac{S_y}{Z_y}\right)\left(\frac{b_f/2t_f - 0.38\sqrt{E/F_y}}{0.45\sqrt{E/F_y}}\right)\right]$

There is an inconsistency in the AASHTO Equations presented. Where $M_{py} = 1.5S_yF_y$ for HP sections, the equation for non-compact flanges implies a calculated reduction (the term in square brackets) to M_{py} calculated as $M_{py} = Z_yF_y$. It is believed that, for the sake of continuity, the noncompact equation for HP sections should be interpreted as follows:

$$M_n = 1.5S_yF_y\left[1-\left(1-\frac{S_y}{Z_y}\right)\left(\frac{b_f/2t_f - 0.38\sqrt{E/F_y}}{0.45\sqrt{E/F_y}}\right)\right] \quad (2)$$

Without this amendment, the effect of increasing F_y on the computed value of M_{ny} may be greater than the increase in F_y itself since $Z_y/S_y > 1.5$ for all HP sections. PennDOT SOL 483-14-04 Table 6.15.2-1 sets $M_{ry} = 1.5S_yF_y$ regardless of slenderness. This may be non-conservative for piles having non-compact flanges.

1.3.5 Strong axis flexural resistance of H-piles

AASHTO LRFD/DM-4 §6.12.2.2.1 refers to §6.10 for calculation of strong axis flexural resistance, M_{nx}. Calculations for M_n are found in §A6.3.2.

Flange slenderness				$\boldsymbol{M_{nx}}$
		36 ksi	50 ksi	
Compact flange	$b_f/2t_f \le 0.38\sqrt{E/F_y}$	10.8	9.2	$M_{nx} = M_{px} = Z_xF_y$
Noncompact flange	$b_f/2t_f \le 0.83\sqrt{E/F_y}$	23.6	20.0	From AASHTO LRFD Eq. A6.3.2-2: $M_n = Z_xF_y\left[1-\left(1-\frac{0.7S_x}{Z_x}\right)\left(\frac{b_f/2t_f - 0.38\sqrt{E/F_y}}{0.45\sqrt{E/F_y}}\right)\right]$

PennDOT SOL 483-14-04 Table 6.15.2-1 sets $M_{nx} = Z_xF_y$ for compact and $M_{nx} = S_xF_y$ for non-compact sections. This may be non-conservative for piles having non-compact flanges since the reduction factor in the brackets of AASHTO Eq. A6.3.2-2 is often less than the typical ratio S_x/Z_x. This effect is more significant for those sections having reduced section dimensions.

1.3.6 Reduced cross sections due to assumed effect of corrosion

DM-4 §6.15.3.2 requires that when COM624P or LPILE are used to design vertical H-pile foundations that prescribed pile capacities (DM-4 Tables 6.15.3.2P-1 and 6.15.3.2P-2) be used. Table 6.15.3.2P-2 provides values for piles assume to have 1/16 in. section loss resulting from corrosion. The section loss is from all exposed steel and therefore affects geometric dimensions (defined by AISC 2012) as indicated below:

- Dimensions that are reduced 1/8 in.: d, t_w, b_f, t_f
- Dimensions that are reduced 1/16 in.: k, k_1
- Dimension having no change: T

Geometric properties are then calculated using the reduced dimensions. In this study the geometric properties of the gross cross section are those reported in the *AISC Steel Construction Manual* (2012) Table 1-4. Calculation of reduced properties neglects the area of the fillets at the web-flange interface. The loss of section area affects the slenderness of the sections as indicated previously in Table 3. Increasing F_y from 36 to 50 ksi results in two HP sections becoming slender for axial load and three additional HP sections becoming noncompact for flexure. When considering reduced sections, two HP sections are slender for F_y = 36 ksi and two additional HP sections at F_y = 50 ksi. Regardless of strength, all sections are noncompact for flexure when the reduced section is considered.

1.3.7 Capacity of standard HP sections

Based on the calculations presented above, Table 6 shows the impact of increasing F_y from 36 ksi to 50 ksi and the impact of the 1/16 in. section reduction on the nominal strengths P_n, M_{nx} and M_{rny} of the nine standard pile shapes provided in DM-4 Table 6.15.3.2P-1. The proportional impact is the same, regardless of consistent load case (driving condition, etc.) used.

Table 6 Impact of increasing Fy from 36 ksi to 50 ksi and prescribed 1/16 in. section reduction on axial and flexural capacities of HP sections**.**

HP	F_y	P_n			M_{nx}			M_{ny}		
		Gross	Reduced	P_{nr}/P_{ng}	Gross	Reduced	M_{nxr}/M_{nxg}	Gross	Reduced	M_{nxr}/M_{nxg}
	ksi	kips	kips		kip-ft	kip-ft		kip-ft	kip-ft	
14x117	36	1238	1034	0.84	582	485	0.83	268	222	0.83
	50	1720	1436	0.84	806	636	0.79	371	292	0.79
	50/36	1.39	1.39		1.38	1.31		1.38	1.32	
14x102	36	1084	878	0.81	507	388	0.76	231	178	0.77
	50	1505	1219	0.81	671	501	0.75	307	231	0.75
	50/36	1.39	1.39		1.32	1.29		1.33	1.30	
14x89	36	940	738	0.79	423	302	0.71	193	139	0.72
	50	1305	983	0.75	550	384	0.70	252	178	0.70
	50/36	1.39	1.33		1.30	1.27		1.31	1.28	
14x73	36	770	524	0.68	317	201	0.63	145	93	0.64
	50	1039	657	0.63	404	244	0.60	186	114	0.61
	50/36	1.35	1.25		1.27	1.21		1.28	1.23	
12x84	36	886	713	0.81	360	288	0.80	156	124	0.80
	50	1230	991	0.81	500	377	0.75	216	163	0.76
	50/36	1.39	1.39		1.39	1.31		1.38	1.31	
12x74	36	785	615	0.78	315	235	0.75	137	102	0.74
	50	1090	854	0.78	424	304	0.72	185	132	0.72
	50/36	1.39	1.39		1.35	1.29		1.35	1.29	
12x63	36	662	492	0.74	257	170	0.66	111	74	0.67
	50	920	644	0.70	335	215	0.64	145	94	0.65
	50/36	1.39	1.31		1.30	1.26		1.31	1.27	
12x53	36	558	356	0.64	202	117	0.58	87	51	0.59
	50	767	446	0.58	259	142	0.55	112	63	0.56
	50/36	1.37	1.25		1.28	1.21		1.29	1.24	
10x57	36	605	462	0.76	200	149	0.75	89	66	0.75
	50	840	642	0.76	277	195	0.70	123	87	0.70
	50/36	1.39	1.39		1.39	1.31		1.38	1.32	

HP sections are inherently stocky (compact); thus, although a few sections go from being compact to noncompact for flexure or become slender for axial loads, the effects are marginal. For sections that are compact for both F_y = 36 and 50 ksi, the ratio of capacities between members having these strengths is 50/36 = 1.39. For noncompact or slender shapes, this ratio falls. The lowest value of this ratio for the gross sections considered is 1.27 for an HP 14x73

which is also the least compact of the members considered having $b_f/2t_f$ = 14.44. Similarly, for reduced sections, a value of 1.21 is found for an HP 12x53 having $b_f/2t_f$ = 19.23. Although two sections are classified as slender for axial load, HP 14x73 and HP 12x53, the 'degree of slenderness' has little effect on the axial capacity. The value of the reduction factor accounting for slender compression elements, Q_s for these gross sections having F_y = 50 ksi is 0.97 and 0.99, respectively. Capacity reductions associated with the 1/16 in. section reduction range from to 0.55 to 0.84.

1.4 PENNDOT EXPERIENCE AND PRACTICE

PennDOT Pub 15A (1989) is the only parametric study conducted by PennDOT comparing results of wave equation analyses with actual load test data. This study considered different pile hammers, pile sizes, pile lengths, hammer efficiencies and soil damping factors. This 1989 study is believed to be out of date as it used empirical data from actual load tests and maximum compressive stresses were unknown (Forscht 2012). Pub 15A reports 52 H-pile tests. Based on Pub 15A, WEAP input parameters were determined (Table 7) and are included in DM-4 §D10.7.3.8.4. The DM-4-recommended values have been revised marginally since 1989 as shown in Table 7.

Table 7 GRLWEAP input variables used by PennDOT.

GRLWEAP Parameter	Pub 15A (1989)	DM-4 (2012)	Forscht (2012)
Shaft quake	0.10 in.	0.10 in.	0.10 in.
Toe quake	0.10 in.	0.05 in.	0.05 in.
Shaft damping	0.05 sec./ft	0.05 sec./ft	0.05 sec./ft
Toe damping	0.20 sec./ft	0.10 sec./ft	0.10 sec./ft
Shaft percentage	10%	10%	30%[a]
Hammer pressure	100%	100%	100%
[a] recommendation to increase shaft percentage to 20% for one year and evaluate further increase to 30% thereafter.			

Forscht (2012) reported a study initiated because PennDOT's standard procedure for performing WEAP (using GRLWEAP) did not consistently provide results in agreement with CAPWAP results based on actual PDA input for point and end bearing piles. The objective of the study was to identify parameters within GRLWEAP that may be modified to improve this agreement. The study considered 41 PDA data obtained from 12 projects. The data included four pile shapes (10x57 (n = 13), 12x74 (n = 13), 12x84 (n = 3) and 14x117 (n = 12)) and five hammer types (Pileco D19-42, ICE I-46, Berminghammer B-21, ICE I-30 and ICE I-19). Table 7 summarizes the GRLWEAP parameters recommended based on Pub 15A, those prescribed by DM-4 (2012) §D10.7.3.8.4, and those recommended by Forscht.

Forscht concluded that although quake and damping parameters affect GRLWEAP output, they do so in an inconsistent manner and only values determined *post priori* improve predictive results of WEAP; thus no change to the DM-4-prescribed values was recommended. Similarly, reducing hammer pressure to 80% had negligible effects on GRLWEAP output (Forscht 2012).

Increasing the shaft percentage from 10% to 30% was found to reduce the GRLWEAP overestimation of CAPWAP-determined maximum compressive stress. The degree of improvement was greater for larger pile sizes although this reflects the greater overestimation of stress for the larger piles. Table 8 summarizes representative results presented by Forscht based on pile size and hammer type. The data reported in Table 8 was obtained from "Executive Table 1" in Forscht (2012) and has been updated to correct apparent reporting errors in the original report (revised data provided by Watral 3.12.15).

Table 8 Maximum compressive stress determined in field and predicted by GRLWEAP for five example cases (Forscht 2012).

Designation	**TP-2**	**B3**	**P5**	**TP-12**	**3054**
Pile size	12x74	10x57	12x74	14x117	14x117
Hammer	ICE I-19	Pileco D19-42	Pileco D19-42	ICE I-30	Pileco D19-42
In situ maximum compressive stress	24.4 ksi	26.2 ksi	24.0 ksi	25.5 ksi	24.9 ksi
GRLWEAP with 10% shaft friction	32.7 ksi	41.6 ksi	33.4 ksi	43.9 ksi	37.7 ksi
GRLWEAP overestimation of in situ stress	34%	59%	39%	72%	51%
GRLWEAP with 30% shaft friction	30.1 ksi	33.4 ksi[1]	27.4 ksi	34.6 ksi	29.7 ksi
GRLWEAP overestimation of in situ stress	23%	27%	14%	36%	19%

[1] revised per Watral, 3.12.15.

Forscht (2012) recommend increasing the shaft friction percentage to 30% in GRLWEAP analyses in order to better replicate results observed in the field. Increasing this parameter in

GRLWEAP will lead to larger pile hammer stroke values being approved for use and therefore more efficient pile driving operations. Forscht continues to recommend limiting pile stresses to 32.4 ksi ($0.9F_y$) and 40 ksi ($0.8F_y$) for 36 ksi and 50 ksi piles, respectively. Subsequently, SOL 483-13-12 revised the limiting pile stress to $0.9F_y$ regardless of yield strength.

Watral (2013) reports a limited evaluation of the geotechnical capacity of H-piles in weak or soft rock – identified as weak shale – in order to assess the implications of the use of 50 ksi (rather than 36 ksi) H-piles. Watral considered four data sets from Pub 15A: sheets 18, 23, 27 and 30; these are summarized along with Watral's findings in Table 9. For each case, a WEAP analysis (using GRLWEAP) based on 'current methodology' (2013) was followed by a static analysis using actual soil profiles. For F_y = 36 ksi, the piles did not appear to overstress the rock strata nor exceed the service settlement limit of 1 inch in any case (this is expected), although the analyses revealed some issues with the data reported in Pub 15A.

Table 9 Summary of H-pile capacity in weak shale (Watral 2013).

Pub 15A sheet no.	**18**	**23**	**27**	**30**
Pile size	12x74	10x57	12x74	12x74
Hammer type	ICE-640	LB 520	LB 520	ICE-640
Hammer rated energy	40000 ft-lbs	26300 ft-lbs	26300 ft-lbs	40000 ft-lbs
Pile embedment	61.0 ft	31.5 ft	33.5 ft	35.5 ft
Ultimate capacity from static load test (Pub 15A)	524 kips 24.0 ksi	340 kips 20.2 ksi	290 kips 13.3 ksi	480 kips 22.0 ksi
Total settlement at ultimate capacity (Pub 15A)	1.02 in.	0.67 in.	0.45 in.	0.60 in.
WEAP capacity	575 kips 26.4 ksi	376 kips 22.4 ksi	340 kips 15.6 ksi	550 kips 25.2 ksi
Static analysis capacity	655 kips 30.0 ksi	376 kips 22.4 ksi	298 kips 13.7 ksi	548 kips 25.1 ksi

The tests reported in sheets 18, 23 and 27 were stopped at displacements of 1 in. or less. This is inadequate to ensure that the bedrock is fully engaged. For example, calibrating the pile tip displacement (0.60 in.) with the static load test results, yield a static modulus of weak shale of only E_s = 1884 ksf, well below the typical minimum value for weak shale of 3000 ksf. This result, like those reported on sheets 23 and 27, indicate a test result dominated by pile friction rather than bearing capacity. Watral reports that the 61 ft pile embedment for sheet 18 was too long to adequately assess tip capacity. Additionally, sheets 23 and 27 report smaller hammers were used than would be used for production piles.

The test reported based on sheet 30 therefore provided the basis for most of Watral's conclusions. In this case the modulus of the weak shale was computed to be E_s = 10,490 ksf, an appropriately sized hammer was used and the bearing test was carried out to 1.45 in. (resulting in an ultimate capacity of 570 kips (26 ksi).

Watral concluded that the net settlement limit of 1.0 in. (DM-4 §D10.5.2.2) does not allow for adequate development of the shaft friction or pile tip bearing resistance to develop the required ultimate geotechnical resistance. This was observed for 36 ksi piles in weak shale. When considering 50 ksi piles, either the pile capacity will increase for the same pile size or the pile size will decrease for the same applied load. In either case, the pile shortening component of settlement will increase. In theory, the pile shortening component will increase by the ratio of capacity increase for the same pile size or by the inverse of the pile area decrease for the same applied load. Watral recommends revising §D10.5.2.2 to increase the pile foundation settlement limits from 1.0 to 1.5 in. Based on the limited scope of the study, this recommendation should only be applied to 'weak rock' conditions. It is unlikely to be an issue for stronger rock. Watral additionally cites the '8% rule-of-thumb' as further support for increasing the settlement limit to

1.5 in. Finally, Watral recommends more refined reporting of geotechnical data for weak rock in order to more accurately assess settlement values.

1.4.1 I-95/I-276 Interchange pile testing program (PTC 2011)

The Pennsylvania Turnpike Commission (PTC 2011) reports a pile testing program undertaken as part of the I-95/I-276 Interchange Project. Of the eight piles tested, six were H-piles: three 12x74 and three 14x89 (Table 10). All piles were reported to be ASTM A-572 Grade 50 steel having a nominal yield strength, F_y = 50 ksi. All piles were driven to absolute refusal, defined as 20 blows per inch in soft or decomposed rock, or dense or hard soil strata.

The objectives of the study were to a) evaluate the capacity of pile drivability into a thick saprolite layer; b) determine the ultimate geotechnical capacity of the piles specifically to determine whether geotechnical or structural capacity controls the design; c) identify if varying saprolite thickness affects the ultimate capacity; and d) monitor ground surface vibration associated with pile driving. Objective b) is the primary concern relative to the present study.

PennDOT and the PTC independently own and designed the interchange structures. PennDOT-owned structures were designed according to DM-4 §6.15.1 which at the time limited the yield strength for steel to be used in structural pile design to 36 ksi. PTC's Design Guidelines allow for the use of 50 ksi. This situation permits a direct comparison of piles designed using the different provisions (Table 10). Although the report focuses on reduced section capacity (accounting for eventual 1/16 in. section loss due to corrosion), only full section capacity, defined as $0.35F_yA$, is presented in Table 10.

PDA monitoring and subsequent CAPWAP analyses were conducted at the end of initial driving (EOID) and at the beginning of restrike (BOR). In all but pile TP-1, BOR capacities are

greater than EOID capacities; only the greater value is reported here. In all cases, the PDA-determined driving stresses were below the allowable driving stress of $0.8F_y$ = 40 ksi (Table 10). It is noted that subsequent revision by SOL-13-12 increases this limit to $0.9F_y$ = 45 ksi. Both Case Method (Goble et al. 1980) and CAPWAP analyses were performed to determine the pile capacities. The resulting factored (ϕ = 0.65) geotechnical pile capacities all exceed the structural capacities; indicating that regardless of pile yield strength, the structural capacity controls design in these cases.

All piles penetrated a first saprolite layer (SPT > 40 blows for 12 in.) and embedded into a second denser layer (SPT > 50 blows for 6 in.). Piles TP-3 and TP-3B were founded on rock while the others were driven to refusal (20 blows per inch) within the second saprolite layer. A function of the saprolite embedment, with the exception of TP-1, skin friction percentage was predicted (using CAPWAP) to exceed 30% in all cases supporting the primary conclusion of Forscht (2012).

Table 10 Pile test details and results from PTC Pile Test Program (PTC 2011).

Test	**TP-1**	**TP-1B**	**TP-2**	**TP-2A**	**TP-3**	**TP-3B**
Pile size	12x74	14x89	12x74	14x89	12x74	14x89
Pile embedment	36.0 ft	33.9 ft	45.0 ft	44.5 ft	57.0 ft	55.0 ft
Design structural capacity: F_y = 36 ksi	275 kips	329 kips	275 kips	329 kips	275 kips	329 kips
Design structural capacity: F_y = 50 ksi	382 kips	457 kips	382 kips	457 kips	382 kips	457 kips
Max. driving stress (from PDA)	38.2 ksi	33.4 ksi	36.1 ksi	37.0 ksi	38.3 ksi	32.7 ksi
Factored geotechnical capacity (Case)	477 kips	498 kips	473 kips	551 kips	506 kips	499 kips
Factored geotechnical capacity (CAPWAP)	449 kips	472 kips	468 kips	530 kips	474 kips	468 kips

1.5 GEOTECHNICAL RESISTANCE OF DRIVEN PILES

The geotechnical resistance of a driven pile is the ultimate capacity of the supporting soil and/or rock layers for carrying the design load. For an end-bearing pile, the ultimate geotechnical capacity is the sum of the tip bearing resistance and skin friction of the pile. Adequate geotechnical data is required to ensure an accurate estimation of the geotechnical resistance of a pile. According to AASHTO LRFD §10.4.2, an extensive subsurface exploration of the soil deposits and/or rock formations is needed to analyze foundation stability and settlement. A subsurface study should contain information about the: present geotechnical formation(s), location and thickness of soil and rock units, engineering properties of soil and rock units (such as unit weight, shear strength and compressibility), groundwater conditions, ground surface topography, and local considerations (such as liquefiable, expansive or dispersive soil deposits, underground voids from weathering or mining activity or slope instability). Empirical or semi empirical static analysis methods are used to determine the ultimate axial capacity of a single pile and pile group. Static analysis methods use the soil strength and compressibility properties to determine pile capacity and performance from which the number of piles and pile lengths may be determined.

There are different static analysis methods introduced for determining the nominal bearing resistance of piles. PennDOT DM-4 §10.7.3.8.6 prescribes the use of methods such as: α – method, β – method, λ – method, Nordlund/ Thurman method, and the SPT or CPT methods. Hannigan et al. (2006) classifies the use of different static analysis methods for cohesionless and cohesive soils.

1.5.1 AASHTO LRFD/DM-4 §10.7.3.8.6 – Pile bearing resistance

The factored pile bearing resistance, $R_{R,}$ is the sum of the pile tip and side resistances:

$$R_p = \phi R_n = \phi_{stat} R_p + \phi_{stat} R_s \quad (3)$$

Where R_p = pile tip resistance: $R_p = q_p A_p$

R_s = pile side resistance: $R_s = q_s A_s$

In which q_p and q_s are the unit tip and side resistances, respectively; and A_p and A_s are the area of the pile tip and the surface area of the pile side, respectively. ϕ_{stat} is the resistance factor for the bearing resistance of a single pile specified in DM-4 Table 10.5.5.2.3-1 (repeated here as Table 11).

Table 11 Resistance factors for single driven piles, ϕ_{stat} (DM-4 Table 10.5.5.2.3-1).

Clay or mixed soils	α -method	$\phi_{stat} = 0.70$
	β -method	$\phi_{stat} = 0.50$
	λ -method (Vijayvergiya & Focht 1972)	$\phi_{stat} = 0.55$
Sandy soils	Nordlund/Thurman Method	$\phi_{stat} = 0.50$
	SPT-method	$\phi_{stat} = 0.45$
	CPT-method	$\phi_{stat} = 0.55$

1.5.2 Static analysis methods for determining nominal bearing resistance of piles in cohesionless soils

The nominal bearing capacity of piles in cohesionless soils depends on the relative density of the soil. The driving forces increase the relative density of the soil around the pile-soil interface and, as a result, the bearing capacity of the pile increases. The type of pile has an impact on the relative density of soil: piles with large displacement (precast concrete piles) increase the relative

density of cohesionless material more than low displacement steel H-piles (Hannigan et al. 2006). The different static methods promulgated by DM-4 for cohesionless soils are summarized below and the related capacity equations are presented in Table 12.

β – Method – This method is used to calculate the bearing resistance of piles in cohesionless, cohesive, and layered soils. This is an effective-stress based method which is developed to model long term drained shear strength conditions.

λ – Method - This method estimates the undrained skin friction considering the length of a pile incorporating both the effective overburden stress and the undrained shear strength of the soil. This method relates the unit skin resistance to short term passive earth pressure.

Nordlund Method – This method is based on field observations and considers the shape of pile taper and its soil displacement in calculation the shaft resistance. The method also accounts for the differences in soil-pile coefficient of friction for different pile materials. The method is based on the results of several load test programs in cohesionless soils. The piles used to develop the method's design curves had widths in the range of 10-20 inches. The Nordlund method tends to over-predict pile capacity for piles with widths greater than 24 inches.

Meyerhof Method – This method is based on standard penetration test (SPT) data

Nottingham and Schmertmann Method – This method is based on the Cone Penetration Test (CPT) data and it is used for both cohesive and cohesionless soils.

1.5.3 Static analysis methods for determining nominal bearing resistance of piles in cohesive soils

The bearing resistance of a pile in cohesive soil is the sum of the tip resistance and skin friction (or shaft resistance). However the shaft resistance of piles driven in cohesive soils is frequently

as much as 80 to 90% of the total capacity. The pile design load should be supported by soil resistance developed only in soil layers that contribute to long term load support. The soil resistance from soils subjected to scour, or from soil layers adjacent soft compressible soils should not be considered (Hannigan et al. 2006). The different static methods promulgated by DM-4 for cohesive soils are summarized below and the related capacity equations are presented in Table 13.

α – Method - This is a total stress method used to calculate the ultimate capacity of undrained cohesive soil using the shear strength of the soil. This method assumes that the shaft resistance is independent of the effective overburden pressure.

β – Method – This method is used to calculate the bearing resistance of piles in cohesionless, cohesive, and layered soils. This is an effective-stress based method which is developed to model the long term drained shear strength conditions.

Nottingham and Schmertmann Method – This method is based on the Cone Penetration Test (CPT) data and it is used for both cohesive and cohesionless soils.

1.5.4 Nominal bearing capacity of piles on rock

Pile foundations on rock are designed to support large loads. The determination of load capacity of driven piles on rock should be made on the basis of driving observations, local experience and load tests. Driving observations are meant to verify the practicality of gaining the desired penetration into rock. Except for soft weathered rock, the structural capacity of the pile will generally be lower than the capacity of rock to support loads for toe bearing piles on rock of fair to excellent quality; therefore the allowable design stress for the pile material will govern the pile capacity in many cases (Hannigan et al. 2006).

According to AASHTO LRFD/DM-4 §10.7.3.2.2, piles supported on soft rock should be designed in a manner similar to piles supported on soils and the bearing resistance should be estimated as described in §10.7.3.8 or by geotechnical analysis to determine the limiting resistance as either the structural resistance or the geotechnical resistance. Revision to DM-4 C10.7.3.2.2 defines “soft or weak rock” as rock having uniaxial compressive strength less the 500 tsf (6.95 ksi).

Table 12 Summary of static analysis methods for piles in cohesionless soils

Method	AASHTO (2010) NHI-05-042 (2006)	Tip resistance	Side resistance	Parameters
β– Method	10.7.3.8.6c 9.7.1.3	$q_p = N_p\sigma'_p$	$q_s = \beta\sigma'_v$	N_p = tip bearing capacity coefficient σ'_p = effective overburden pressure at the pile tip β = an empirical coefficient σ'_v = vertical effective stress
λ - method	10.7.3.8.6d	-	$q_s = \lambda(\sigma'_v + 2S_u)$	S_u = undrained shear strength $(\sigma'_v + 2S_u)$ = passive lateral earth pressure λ = an empirical coefficient
Nordlund/ Thurman method	10.7.3.8.6f 9.7.1.1c	$q_p = \alpha_t N'_q \sigma'_v \leq q_L$	$q_s = K_\delta C_F \sigma'_v \frac{\sin(\delta+\omega)}{\cos\omega}$	α_t = coefficient N'_q = bearing capacity factor q_L = limiting unit tip resistance K_δ = coefficient of lateral earth pressure at mid-point of soil layer C_F = correction factor for K_δ when $\delta \neq \phi_f$ ω = angle of pile taper from vertical δ = friction angle between pile and soil
Meyerhof Method (ksf units)	10.7.3.8.6g 9.7.1.1a	$q_p = \frac{0.8(N1_{60})D_b}{D} \leq q_L$	$q_s = \frac{\overline{N1}_{60}}{50}$	$N1_{60}$ = representative SPT blow count near pile tip D = pile width or diameter D_b = depth of penetration in bearing strata q_L = limiting tip resistance taken as $8N1_{60}$ for sands and $6N1_{60}$ for nonplastic silt (ksf)
Nottingham Method	10.7.3.8.6g 9.7.1.7b	$q_p = 0.5(q_{c1}+q_{c2})$	$R_s = K_{s,c}\left[\sum_{i=1}^{N1}\left(\frac{L_i}{8D_i}\right) f_{si}a_{si}h_i + \sum_{i=1}^{N2} f_{si}a_{si}h_i\right]$	q_{c1} = average static cone tip resistance over a distance yD below the pile tip q_{c2} = average static cone tip resistance over a distance $8D$ above the pile tip $K_{s,c}$ = correction factor for clays and sands L_i = depth to middle of length interval i D_i = pile width or diameter f_{si} = unit sleeve friction resistance from CPT a_{si} = pile perimeter h_i = length interval N_1 = intervals between ground surface $8D$ below ground surface, and N_2 = intervals between $8D$ below ground surface and pile tip

Table 13 Summary of static analysis methods for piles in cohesive soils.

Method	AASHTO LRFD (2010) NHI-05-042 (2006)	Pile tip resistance	Pile side resistance	Parameters
α – method	10.7.3.8.6b 9.7.1.2a	$q_p = 9S_u$	$q_s = \alpha S_u$	α = adhesion factor applied to S_u S_u = undrained shear strength
β – Method	10.7.3.8.6c 9.7.1.3a	$q_p = N_p\sigma'_p$	$q_s = \beta\sigma'_v$	N_p = tip bearing capacity coefficient σ'_p = effective overburden pressure at the pile tip β = an empirical coefficient σ'_v = vertical effective stress
Nottingham-Method	10.7.3.8.6g 9.7.1.7b	$q_p = 0.5(q_{c1}+q_{c2})$	$R_s = \alpha' f_{si} A_s$	q_{c1} = average static cone tip resistance over a distance yD below the pile tip q_{c2} = average static cone tip resistance over a distance $8D$ above the pile tip α' = Ratio of pile shaft resistance to cone sleeve friction A_s = pile-soil surface area over f_{si} depth interval

1.5.5 Minimum pile penetration

Minimum penetration length is intended to ensure that all the limit state requirements are fulfilled. According to AASHTO LRFD §10.7.6 minimum pile penetration length is the maximum penetration required to meet: settlement and lateral deflection under service limit state; uplift, penetration into bearing soils below downdrag and soil subject to scour, minimum depth of fixity under strength limit state; and uplift and lateral resistance under extreme events.

1.6 DYNAMIC ANALYSIS OF PILES (WEAP)

Wave equation analysis of pile driving (WEAP) is a numerical method for assessing the driving behavior of driven piles. WEAP predicts the pile capacity versus blow count relationship, the so called bearing graph, and pile driving stress. A WEAP model represents the pile driving hammer and its accessories (ram, cap, and cap block) and the pile, as a series of lumped masses and springs in a one-dimensional analysis. The soil response for each pile segment is modeled as being viscoelastic-plastic. The conceptual one-dimensional WEAP model is shown in Figure 1.

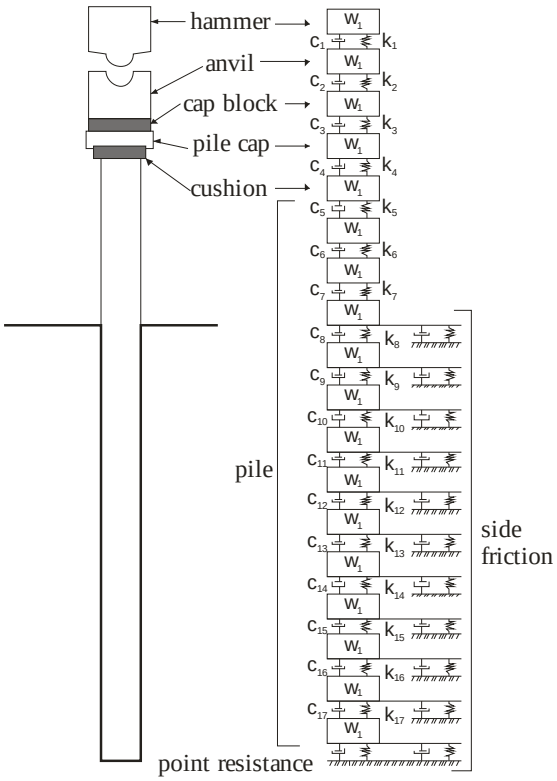

Figure 1 Conceptual representation of WEAP analysis.

WEAP analyses are often used to conduct drivability analyses to select parameters for safe pile installation, including recommendations on cushion stiffness, hammer stroke and other driving system parameters that optimize blow counts and pile stresses during pile driving. For a single hammer blow, a WEAP analysis may (Lowery 1993):

1. Predict the driving stresses induced in the pile
2. Determine the resulting motion of the pile
3. Determine the resistance to penetration afforded by the soil

With this information, the following engineering questions may be addressed (Lowery 1993):

1. Can the given hammer drive the pile to the required depth?
2. What rate of penetration will be provided; i.e.: how long will it take to drive the pile?
3. What is the maximum penetration that may be achieved?
4. Will excessive stresses occur in the pile during driving?

The primary objective of a dynamic analysis, relevant to this study, is to determine whether a pile is overstressed when driven to a capacity equal to the factored axial resistance increased by a resistance factor. For this purpose, the present study will use GRLWEAP software (PDI 2010). The WEAP analysis requires as input information regarding the hammer, pile, and soil column.

The steps involved in a WEAP analysis are the following (FHWA 2003):

1. Determine the pile length.
2. Determine the distribution and magnitude of side friction.
3. Determine damping factors: Case or Smith skin damping, skin quake for soils and rocks.
4. Hammer selection, helmet and cushion properties.
5. Permissible driving stress.
6. Compute ultimate capacity and maximum driving stress.

In an analysis, the major engineering effort lays in steps (2) and (3). These steps require the incorporation and interpretation of geotechnical information. Not only is it necessary to calculate the static resistance and its distribution; but also additional dynamic soil resistance

parameters, damping and quake, both at the shaft and toe must be estimated. The piles considered in this study will be primarily end bearing but some shaft skin friction may be present during driving. Skin friction will be a parameter of study; values up to 0.30 (based on Forscht 2012) will be considered. GRLWEAP-suggested quake and damping values will be used in this study. Forscht (2012) has confirmed the use of the values recommended in the GRLWEAP manual as listed in Table 14 and Table 15.

Table 14 Recommended quake values for impact driven piles (PDI 2010).

	Soil type	**Pile type or size**	**Quake (in.)**
Shaft quake	All soil types	All pile types	0.10
Toe quake	All soil types, soft rock	Non-displacement piles	0.10
	Very dense or hard soils	Displacement piles having diameter or width D	D/120
	Soils that are not dense or hard		D/60
	Hard rock	All pile types	0.04

Table 15 Recommended damping values for impact driven piles (PDA, 2010).

	Soil type	**Damping factor (s/ft)**
Shaft damping	Non-cohesive soils	0.05
	Cohesive soils	0.20
Toe damping	All soil types	0.15

2.0 PARAMETRIC STUDY METHODS AND MATRIX

The primary result of a WEAP (Wave Equation Analysis of Pile Driving) analysis is a bearing graph which represents the relationship between blow count and pile capacity. It is an efficient tool used to control pile driving. The accuracy of a bearing graph depends on the parameters related to the dynamic hammer – pile –soil system (Figure 1). Input parameters are based on experience and therefore often they cannot perfectly imitate an actual situation. For instance, often the blow count is inaccurate or the soil resistance changes with time which, in the end, will result in a bearing graph with inaccurate data. Therefore knowledge of fundamental characteristics of the mechanics and dynamic interaction of all components involved in the pile driving process is required. The parameters investigated in this study are selected based on the effects that they have on the pile capacity and drivability. The input parameters are categorized as parameters related to: the driving system (hammer); the pile section; and the soil.

The hammer impact on the top of the pile generates an elastic compression wave causing strain (deformation) in the pile and motion of the pile into the soil. The length and initial intensity of the stress wave in the pile depend on: ram weight; hammer stroke; hammer efficiency; hammer and pile cushion stiffness and coefficient of restitution (COR); and helmet weight. Pile physical and mechanical properties also play important roles in pile drivability. The blow count may be twice as high for heavier and stiffer piles.

Damping and quake factors are the two important parameters related to the characteristics of the soil as described in Sections 1.5 and Section 1.6. Damping is analogous to friction which must be overcome when driving a pile and quake quantifies the degree of rebound caused by the soil. Damping effects are more critical in cohesive soils for which higher skin (shaft) damping values are used (see Table 15). For this reason the blow counts required to achieve a desired pile capacity in cohesive soils are higher than those in cohesionless soils (Hussein , Bixler, & Rausche, 2003). On the other hand, soil stiffness is inversely proportional to the quake. The quake factor only varies substantially at the pile toe and is primarily as a function of the volume of soil displaced. Higher bearing capacities with lower blow counts are attained for soils with lower toe quake compared to soils with higher values of toe quake (AASHTO LRFD 2010).

2.1 METHODOLOGY

In this study, the commercially available program GRLWEAP (Version 2010-4) is used for all analysis (see Section 1.6). For each case considered, a two-step analytical approach is used. Each case represents a pile section, pile length, shaft friction and 'target' capacity as described subsequently. Each analysis begins with trial hammer parameters (type, stroke and energy) and iterates upon these until the target capacity is attained at 240 blows/ft – a value defined as 'refusal'. The objective of each analysis is to achieve the target capacity with the smallest (i.e. least energy) hammer (of the five considered; described in Section 2.2.2, below) while still providing at least a 0.5 foot working stroke range. All results are reported with 'one decimal precision'; that is, 0.1 ksi, 0.1 ft and 0.1 kip-ft precision. Capacity is reported to the nearest kip. Each analysis progresses as follows:

Case 1: The pile is driven using a constant hammer stroke analysis such that the following capacities are attained at 240 blows/ft refusal:

a) A_sF_y, representing twice the AASHTO LRFD (2010) design capacity for severe driving conditions; i.e., 2 x $0.5A_sF_y$;

b) $0.66A_sF_y$, representing twice the current DM-4 (SOL 483-14-04) design capacity for severe driving conditions; i.e., 2 x $0.5(0.66A_sF_y)$; and,

c) $0.50A_sF_y$. This case provides 'historic' perspective for 36 ksi piles. That is, twice the design capacity = 2 x $0.35A_s$(36 ksi) = 25.2 ksi ≈ $0.5A_s$(50 ksi).

For each specified capacity the resulting driving stress and hammer parameters (type, stroke, energy) are recorded. The factor 2 in each case represents the required ultimate capacity to which a pile must driven when PDA is not used in the field. In cases where PDA is used to monitor the driving operation, this factor is permitted to be reduced to 1.54 (DM-4, 2014). These analysis cases are referred to as 1a, 1b and 1c.

Case 2: In order to assess maximum potential pile capacity, a fourth case, using the same hammer as used in Case 1a (or Case 1b, or both) in which the pile is driven using a constant hammer stroke analysis such that the driving stress is $0.9F_y$ = 45 ksi at 240 blows/ft refusal is conducted. Resulting pile capacity and hammer parameters are recorded. These cases are referred to a 2a and 2b.

Case 3: Using the same hammer as used in Case 1a, the pile is driven using a constant hammer stroke analysis such that the capacity is $0.66A_sF_y$ ***or*** the driving stress reaches the PennDOT-prescribed lower limit of 25 ksi at 240 blows/ft refusal (DM-4 C6.15.3P). This represents the minimum PennDOT-acceptable capacity to which the pile/hammer case may be driven. From this case, the following data is recorded: [minimum] stroke, pile capacity at refusal

and hammer energy. If the difference in required stroke between cases 2 and 3 does not exceed 0.5 ft, a different hammer will be selected and cases 2 and 3 repeated.

Case 4: Using the same hammer as used in Case 1a, the pile is driven using a constant hammer stroke analysis such that the driving stress is 25 ksi at 240 blows/ft refusal (DM-4 C6.15.3P). From this case, the following data is recorded: [minimum] stroke, pile capacity at refusal and hammer energy.

2.2 PARAMETER SELECTION

The parameters considered in this study are described briefly in the following paragraphs.

2.2.1 Pile section

Three pile sections are selected:

HP 14x117 is a representative heavy section which is compact for axial load at F_y = 50 ksi. Benchmark data available is available from Forscht (2012).

HP 12x74 is a representative medium section and is the most common shape used in PA. Benchmark data is available in Publication 15A, Forscht (2012), PTC (2011) and recent 50 ksi pile driving records.

HP 10x57 is a compact section having capacity at F_y = 50 ksi suitable to ‘replace’ 36 ksi HP12x74 piles; theoretically affecting a weight savings of 17 lbs/ft or 23%.

2.2.2 Hammer types, weights and cushions

Hammer types for inclusion in the analyses were recommended by PennDOT as those readily available to PA contractors; these are summarized in Table 16 and are shown from smallest to largest from left to right across the table. Hammer parameters used in the GRLWEAP analysis are also shown.

Table 16 Hammer parameters used in this study

Hammer		**ICE I-12v2**	**Pileco D19-42**	**ICE I-30v2**	**ICE I-36v2**	**ICE I-46v2**
GRLWEAP ID		1501	852	1504	1505	1506
ram weight	kips	2.82	4.01	6.61	7.94	10.14
maximum stroke	ft	11.45	12.6	12.6	13.1	13.1
rated stroke	ft	10.5	10.6	11.5	11.8	11.8
ram diameter	in.	11.8	12.6	16.5	19.7	19.7
efficiency		0.80	0.80	0.80	0.80	0.80
energy/power	kip-ft	29.6	42.5	76.0	93.7	119.8
fuel setting	psi	1450	1520	1570	1510	1560
Cushion area	in^2	398	398	398	491	491
Cushion modulus	ksi	175	285	175	175	175
Cushion thickness	in.	2.0	2.0	2.0	4.0	4.0
COR		0.91	0.80	0.91	0.91	0.91

2.2.3 Soil types above rock

The ground is composed of layers of soils that support the pile by friction and the bedrock at the bottom that support the pile by bearing. Only hard rock will be considered as bearing strata as this is the most severe driving condition. Non-cohesive soil is considered since this has smaller skin damping, and therefore also represents a more severe driving scenario. Cohesive soils are critical when considering minimum hammer stroke requirements.

2.2.4 Shaft friction

Forscht (2012) recommended using 20% shaft friction, potentially increasing this to 30%. Values of both 20 and 30% are used in the present study.

2.2.5 Pile length

Representative embedded pile lengths of 20, 50 and 80 feet are considered in the analyses. Each pile has 4 feet added to its embedded length facilitate driving.

Table 17 represents a matrix of 126 base scenarios (i.e.: 3 pile shapes x 3 pile lengths x 2 shaft friction values x 7 analysis cases). Additional sensitivity analyses addressing toe damping, toe quake and skin damping are also made on a subset of these base scenarios considering only HP 12x74 piles having an embedded length of 50 ft. Benchmark analyses will also be made as described in Section 2.2.6.

Table 17 Analysis parameter matrix

Parameter	units	values considered in analyses
pile Section		HP 10x57, HP 12x74 and HP 14x117
embedded length	ft	20, 50 and 80 ft
pile length	ft	24, 54 and 84 ft
hammer		smallest hammer of those listed in Table 16 that achieves target capacity at 240 blows/ft
toe damping	sec/ft	0.10 (rock); 0.15 (soil; 50 ft long HP 12 x 74 only)
toe quake	in.	0.05 (hard rock); 0.15 (sift rock; 50 ft long HP 12 x 74 only)
skin damping	sec/ft	0.10 (non-cohesive soil); 0.20 (cohesive soil; 50 ft long HP 12 x 74 only)
skin quake	in.	0.10
shaft friction	%	20 and 30

2.2.6 Benchmark scenarios

Within the proposed parameter scenario matrix it is necessary to establish some benchmark tests – tests for which the PDA/CAPWAP data is available – against which a comparison of analytical data may be made. This will help to validate the GRLWEAP analyses conducted and will permit a refined assessment of shaft friction parameters.

The five analyses presented by Forscht (2012), summarized in Table 8, are essentially contained within the proposed analytic matrix and will be used as benchmarks; these will require additional analysis runs to match pile lengths and hammer types. Similarly, three analyses presented in PTC (2011), summarized in Table 9, are appropriate benchmark candidate data, although these were driven using an ICE-19v2, requiring additional individual analyses to be conducted.

Due to differences in hammers, a direct comparison with Publication 15A data is generally not possible since the hammers reported in Pub. 15A are smaller than those used in the present study. Nonetheless, the data presented on Pub. 15A sheet 18, albeit using an ICE 640 hammer (similar to a Pileco D19-42), may prove an appropriate benchmark case.

Finally, PennDOT has provided some recent pile driving analyses from which benchmarks for 50 ksi design capacity may be obtained. Although having very short pile lengths of 13.5 and 16.5 feet, respectively, TP-439 and TP-440 reported for Abutment 2 of Structure S-33234A (Grindstone Bridge) on SR 4002 are suitable benchmarks for HP 12x74 driven using a Pileco D19-42 hammer.

A summary of benchmark analysis cases, along with their results, is provided in Table 20 at the end of Chapter 3. Each benchmark test will be analysed as indicated and the result compared with the available PDA/CAPWAP data. Values of toe damping (0.10), toe quake

(0.05), skin damping (0.10) and skin quake (0.10) will be the same as those used in the parametric study. As in Forscht (2012), shaft friction will be varied to assess the effect of this parameter and determine the value most closely approximating available data.

3.0 RESULTS OF PARAMETRIC STUDY AND DISCUSSION

This chapter reports the findings of the parametric and benchmark studies described in Chapter 2. The results of the WEAP analyses of all cases are provided in Appendix A. An illustrative example of one series (HP12x74 having L = 54 ft) of output from parametric analysis is provided in Table 18. The shaded entries in each row represent the 'target' values for each analysis as described in Section 2.1.

Table 18 Results of WEAP analysis for HP12x74

Step	Case	Hammer	At 240 blows/ft refusal…					
			Pile capacity			Driving stress	Stroke	Energy
			$1/A_sF_y$	ksi	kips	ksi	ft	kip-ft
1a	HP12x74 (A_s = 21.8 in^2) L = 54 ft SF = 0.20 TD = 0.10; TQ = 0.05 SD = 0.05; SQ = 0.10	ICE 1-36v2	1.00	50.0	1090	62.0	11.81	52.00
1b		Pileco D19-42	0.66	33.0	719	39.0	9.75	23.60
1c		ICE 1-12v2	0.50	25.0	545	30.8	8.66	12.90
2a		ICE 1-36v2	0.73	36.5	800	44.8	8.20	29.90
2b		Pileco D19-42	0.70	35.0	763	41.5	10.60	26.50
3		ICE 1-36v2	0.66	33.0	719	39.5	7.11	23.40
4		ICE 1-36v2	0.43	21.6	466	25.2	4.90	11.30

Based only on the case shown in Table 18, the following is observed:

1. The AASHTO-permitted capacity of the HP12x74 considered, A_sF_y, cannot be reached without significantly exceeding the driving stress limit of $0.9F_y$ = 45 ksi. A driving stress of 62 ksi was predicted. [from case 1a]
2. The SOL 483-14-04-permitted capacity of the HP12x74 considered, $0.66A_sF_y$, can be reached without exceeding the driving stress limit of $0.9F_y$ = 45 ksi. A driving stress of 39 ksi was predicted. [case 1b]
3. The maximum capacity that can be achieved, respecting the driving stress limit of $0.9F_y$ = 45 ksi is $0.73A_sF_y$ = 800 kips (using an ICE I-36v2) or $0.70A_sF_y$ = 763 kips (using an Pileco D19-42) [case s 2a and 2b]. In the latter case, the maximum stroke of the hammer limited the driving capacity and resulted in a maximum driving stress of only 41.5 ksi.
4. Requiring a minimum driving stress of 25 ksi at refusal results in a 'minimum' capacity of $0.43A_sF_y$ = 466 kips [case 4].
5. For the ICE I-36v2 hammer, the limits reported in observations 3 and 4 are found over a stroke range of 4.9 to 8.2 feet (range = 3.3 ft) [case 2a – case 4].
6. The ICE-I-36v2 hammer is shown to satisfactorily drive the pile – meeting, or exceeding a pile capacity of $0.66A_sF_y$ while respecting upper [case 2a] and lower [case 3] driving stress limits and having a stoke between these limits of 1.09 ft (exceeding 0.5 ft) [case 2a – case 3].
7. The Pileco D19-42 hammer is shown to satisfactorily drive the pile – meeting, or exceeding a pile capacity of $0.66A_sF_y$ while respecting upper [case 2b] and lower [case 1b] driving stress limits and having a stoke between these limits of 0.85 ft (exceeding 0.5 ft) [case 2b – case 1b].
8. The change from DM-4 to SOL 483-14-04 provisions resulted in the following [comparing cases 1c and 1b]:

a. A pile capacity increase of 32% (545 to 719 kips).

b. A larger hammer (ICE I-12v2 to Pileco D19-42) being required to drive the pile (energy increase of 77%).

c. A resulting 20.5% increase in pile driving stress (31 to 39 ksi).

Results from all analyses are presented in Appendix A and synthesized in the follow section.

3.1 OBSERVATIONS FROM WEAP ANALYSES

3.1.1 Driving stress

Figure 2 shows the driving stress results for the three HP sections investigated in the parametric study. Each group of six data points are arranged by pile shape and target capacities at refusal (i.e., results of cases 1a through 1c) and are presented in the order indicated in the box at the lower right corner of the Figure.. The dashed lines in the plot show the upper and lower limits for the driving stress; that is, $0.9F_y$ = 45 ksi and 25 ksi, respectively.

The data shown in Figure 2 clearly shows that the driving stress will always exceed ultimate stress. Therefore piles cannot achieve an ultimate stress of A_sF_y when driving stress is limited to $0.9A_sF_y$. However, this does not imply that a design capacity of $0.5A_sF_y$ cannot be achieved, it only requires PDA to accompany driving – in which case the target ultimate capacity is only $0.5A_sF_y/0.65 = 0.77A_sF_y$ rather than $0.5A_sF_y/0.50 = A_sF_y$ when no PDA is used. By the same token, the minimum permissible driving stress of 25 ksi = $0.5A_sF_y$ implies that the minimum drivable ultimate capacity is only somewhat lower than this.

Due to hammer limitations, it was not possible to find a hammer suitable to drive HP14x117 piles having a length greater than 50 ft to a capacity of A_sF_y. Using the largest available hammer (ICE I-46v2), these cases were driven to a capacity between $0.81A_sF_y$ and $0.84A_sF_y$ as indicated in Figure 2 by the solid triangles.

For a given pile section, driving stress decreases with increased pile length. The driving stress also decreases when shaft friction is increased from 0.20 to 0.30. This effect is clearly more pronounced for longer piles and is somewhat more pronounced for larger pile sections due to their greater perimeter dimension.

Due to the need for larger hammers, driving stress increases with pile section. For all piles (except HP14x117 having L = 20 and shaft friction = 0.20) driving stress for piles driven to a capacity of $0.66A_sF_y$ remained below the $0.90A_sF_y$ = 45 ksi limit.

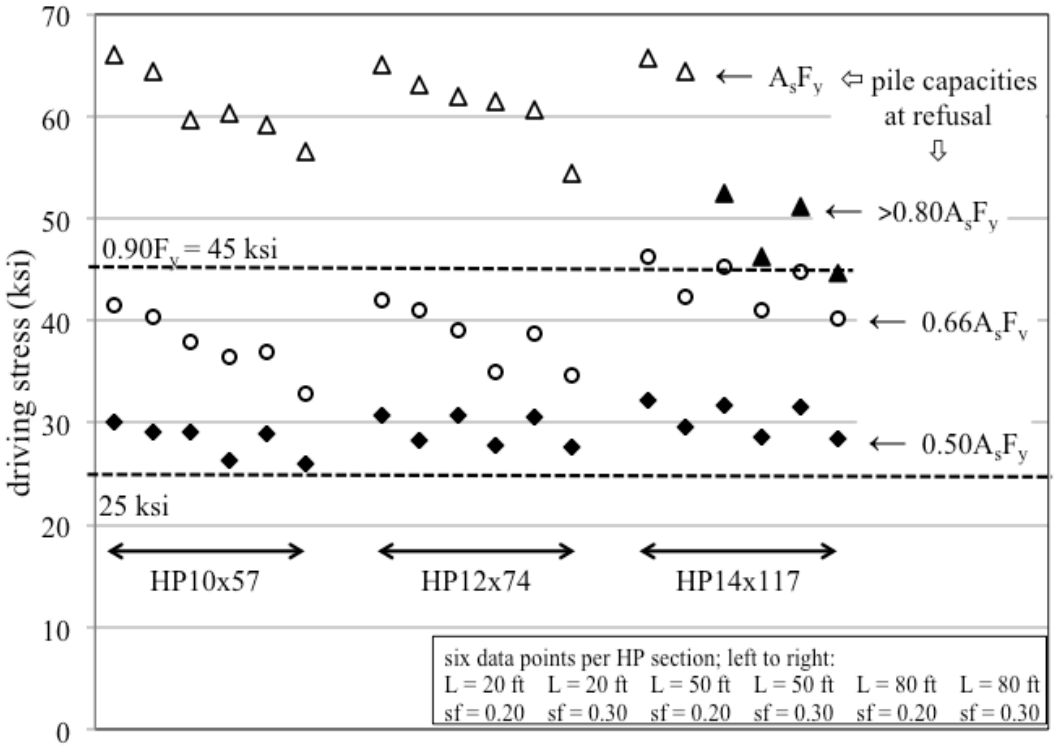

Figure 2 Driving stress distribution

3.1.2 Pile ultimate capacity

Figure 3 shows the range of pile ultimate capacities for the HP sections considered. Using the minimum permitted driving stress of 25 ksi, all pile capacities ultimately fell between $0.40A_sF_y$ and $0.5A_sF_y$ [case 4].

Driving piles to the maximum permitted driving stress of $0.90A_sF_y$ = 45 ksi, resulted in pile capacities ranging from $0.64A_sF_y$ to $0.76A_sF_y$ [case 2b] All HP10x57 piles exceeded $0.70A_sF_y$ and the achievable capacity falls with increasing pile size.

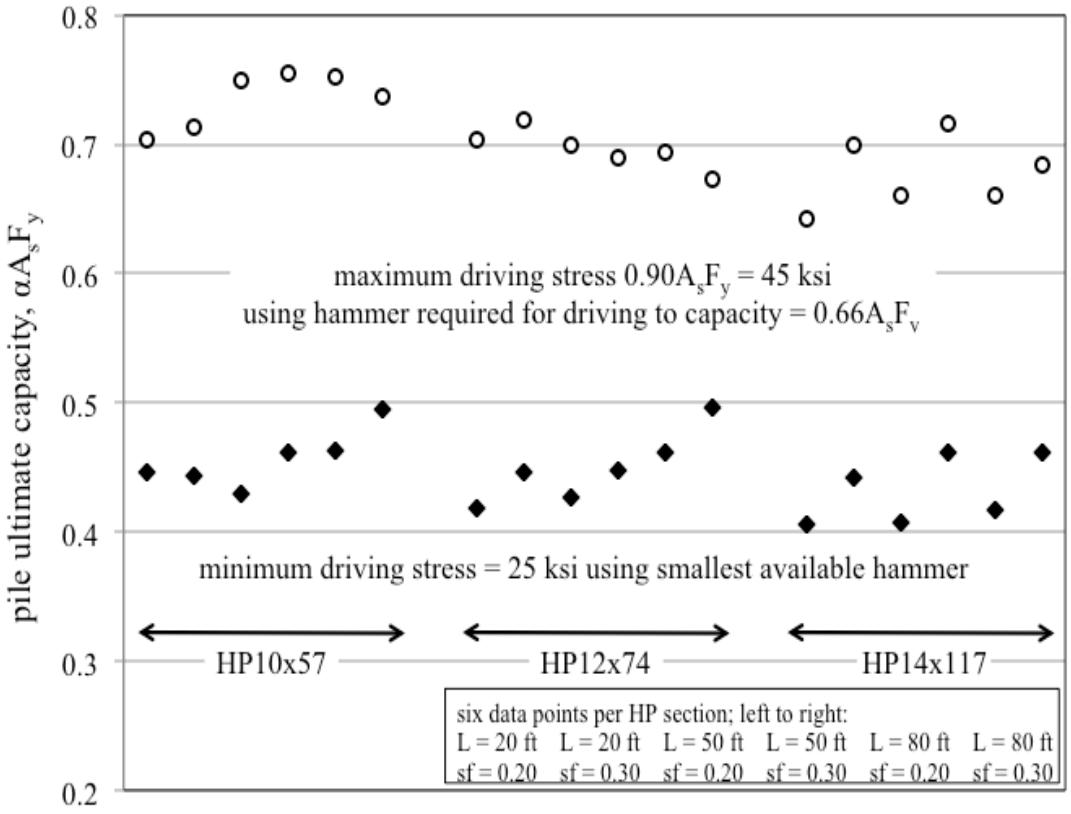

Figure 3 Pile ultimate capacity

3.1.3 Range of hammer stroke

Figure 4 shows the hammer stroke available to drive the piles considered to a capacity of $0.66A_sF_y$ [case 2b – case 1b]. All HP10x57 and HP12x74 piles had available hammer strokes exceeding the recommended limit of 0.5 ft. The available range decreased with increasing pile size. Only HP14x117 piles having shaft friction = 0.30 exhibited hammer stroke ranges exceeding 0.5 ft.

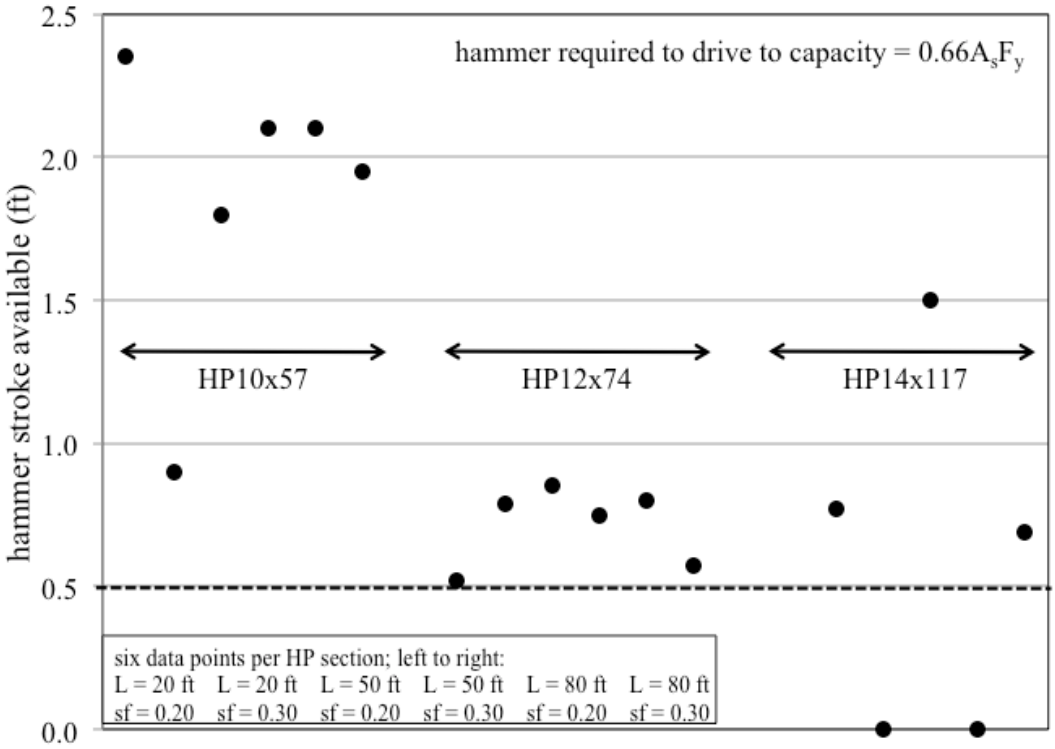

Figure 4 Hammer stroke available

3.1.4 Varying driving parameters

The histogram representation of ultimate pile capacity and driving stress variations obtained by varying selected parameters are shown in Figure 5 and Figure 6, respectively. Four cases are shown for each pile target capacity (horizontal axis):

1. The first case is control case from the primary analysis described above.
2. The second increased shaft damping from 0.05 to 0.20 sec/ft leaving all other parameters the same as the control.
3. The third increases toe damping from 0.10 to 0.15 sec/ft and toe quake from 0.05 in. to 0.10 in. leaving all other parameters the same as the control.
4. The fourth increases shaft damping and toe damping and quake as in the previous cases.

As can be seen in Figure 5, varying the parameters as indicated has little effect on pile ultimate capacity at a given target capacity. Due to reduced driving stresses, piles having shaft damping increased to 0.20 achieved marginally higher ultimate capacities. Driving stresses are also not significantly affected although increasing toe damping and quake increases driving stresses marginally.

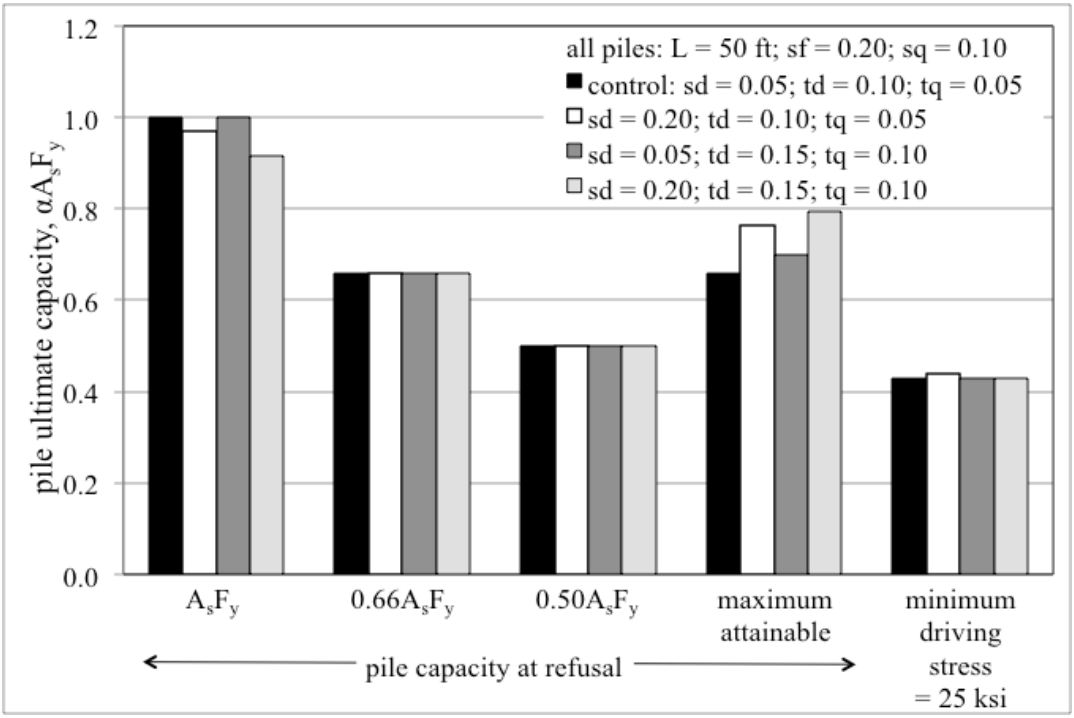

Figure 5 Pile ultimate capacity

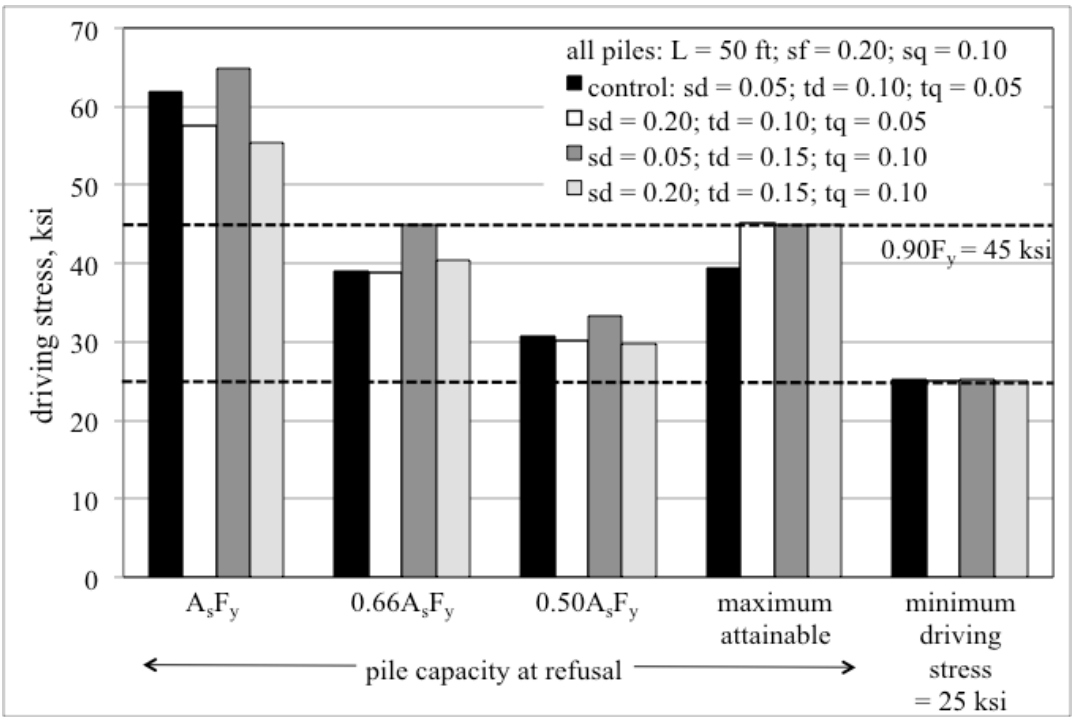

Figure 6 Driving stress

3.1.5 Ratio of driving stress to ultimate stress

Table 19 summarizes and compares the ratio of predicted driving stress to ultimate stress for all analyses conducted. Only data with 20% shaft friction are included.

As described in Section 3.1.1, smaller pile sections require relatively lower driving stresses and therefore allow greater relative capacities to be achieved. Longer pile sections also result in proportionally lower driving stresses.

Given the relatively consistent COV values, these ratios may be used as a rule of thumb for estimating driving stress based on required pile ultimate capacity. Using average values reported in Table 19 and a driving stress limit of $0.9F_y$, HP10x57 sections may be driven to a capacity of $0.76A_sF_y$ (0.9/1.19 = 0.75) while HP14x117 sections would be limited to $0.70A_sF_y$

(0.9/1.29). Using the 'high' value of the ratios, these capacity limits become $0.68A_sF_y$ and $0.65A_sF_y$, respectively.

Table 19 Ratio of driving stress over ultimate stress

Driving stress / ultimate stress	**All shapes considered**				**HP10x57**	**HP12x74**	**HP14x117**
Pile length	All	20 ft	50 ft	80 ft	All	All	All
Average	1.23	1.27	1.22	1.19	1.19	1.21	1.29
COV	0.06	0.05	0.05	0.06	0.05	0.05	0.04
Low	1.07	1.12	1.15	1.07	1.07	1.10	1.20
High	1.40	1.40	1.37	1.36	1.32	1.30	1.40

3.1.6 Conclusions based on present code provisions

1. The AASHTO permitted pile capacity of $0.5A_sF_y$ is not technically achievable without the reduction in required over strength permitted using a PDA (as discussed in Section 3.1.1). Even using a PDA, this capacity may only be achievable for smaller pile sections [case 1a].
2. The SOL 483-14-04 permitted pile capacity of $0.5(0.66)A_sF_y$ in which F_y = 50 ksi is achievable in cases considered although driving stress in the large HP14x117 piles approaches the limit of $0.9A_sF_y$ [case 1b]
3. The theoretical increase in pile capacity realized by accounting for the increase of F_y from 36 to 50 ksi and the revisions to the PennDOT standard is a factor of 1.31. (i.e.: from (0.35 x 36 ksi)A_s to (0.50 x 0.66 x 50 ksi)A_s) This theoretical increase is achievable for all cases considered [compare cases 1c and 1b].
4. For pile sections lighter than HP12x74 having F_y = 50 ksi, the previously (DM-4) prescribed value of $\varphi_c = 0.35$ is achievable.

3.1.7 Benchmark scenarios: GRLWEAP analyses results

Results of GRLWEAP analyses conducted for benchmark scenarios described in Section 2.2.6 are shown in Table 20.

The GRLWEAP analyses for the first five benchmark runs, TP-2, B3, P5, TP-12, and 3054, have been conducted over four cases of shaft friction (10%, 20%, 30% and 40%). The rest of the runs have been analyzed only for one case of shaft friction as shown in Table 20. A ratio of calculated driving stress over field actual driving stress has been estimated for each run in order to compare GRLWEAP predicted driving stress with the actual field stress.

For each benchmark run, the GRLWEAP calculated driving stress matching the actual field driving stress has been highlighted as shown in Table 20. For all of the cases (except TP-12 and Sheet 18 where the inaccuracy of reported field data is assumed) GRLWEAP very accurately predicts the driving stress close to the actual field value for shaft frictions of 20% and 30%.

Table 20 Benchmark scenarios analyses results

ID	HP	A_sF_y	Pile length	Embedded length	Shaft friction	Hammer	Capacity at 240 blows/ft[1]			Calculated driving stress	Calculated Field
							Stress	Capacity	Field driving stress		
		kips	ft	ft	%		1/ A_sF_y	kips	ksi	ksi	
TP-2[a]	12x74	784	40.3	9.1	0.10	ICE I-19V2	0.57	447	26	27.48	1.06
					0.20					26.14	1.01
					0.30					24.93	0.96
					0.40					24.25	0.93
B3[a]	10x57	605	60	44.1	0.10	Pileco D19-42	0.73	440	26.2	32.1	1.23
					0.20					29.2	1.11
					0.30					27.6	1.05
					0.40					26.3	1.00
P5[a]	12x74	784	70.0	38.0	0.10	Pileco D19-42	0.65	509	24	29.6	1.23
					0.20					27.06	1.13
					0.30					24.44	1.02
					0.40					22.06	0.92
TP-12[a]	14x117	1238	65.3	61	0.10	ICE I-30V2	0.83	1024	25.5	44.09	1.73
					0.20					40.26	1.58
					0.30					36.45	1.43
					0.40					32.95	1.29
3054[a]	14x117	1238	100.6	90.1	0.10	Pileco D19-42	0.56	696	24.9	27.24	1.09
					0.20					24.94	1.00
					0.30					22.47	0.90
					0.40					20.08	0.81
TP-1[b]	12x74	1090	60.0	36.0	0.20	ICE I-19V2	0.63	691	38.2	39.75	1.04
TP-2[b]	12x74	1090	65.0	45.0	0.20	ICE I-19V2	0.60	651	36.1	37.12	1.03
TP-3[b]	12x74	1090	65.0	57.0	0.20	ICE I-19V2	0.61	660	38.3	37.59	0.98
Sheet 18[c]	12x74	784	70.0	60.0	0.20	ICE-640	0.33	262	21	14.06	0.67
TP-439[d]	12x74	1090	17.6	13.5	0.30	Pileco D19-42	0.61	662	36.4	38.95	1.07
TP-440[d]	12x74	1090	25.3	16.5	0.30	Pileco D19-42	0.81	883	54.2	49.87	0.92

[1] value reported by source; [a] Forscht (2012); [b] PTC (2011); [c] *Publication 15A* (1989); [d] SR 4005 Abutment 2 (Foundation Testing Services 07.30.2014)

4.0 EXTENDED STEEL H-PILES

4.1.1 Background

There are applications of driven piles as the main supporting elements of the substructure of a bridge, such as pile-bents functioning as a pier system, where driven piles extend out of the ground surface directly supporting the superstructure typically through a precast concrete bent cap. Steel HP shapes, precast concrete piles and concrete-filled steel pipe piles are commonly used as extended or partially embedded driven piles in pile-bent systems. Steel H-piles are very common in North American practice (see Figure 7).

a) Union Pacific Railway over Feather Creek, Yuba County CA (www.bphod.com)

b) *Connection details for PBES: Case Study 3* (www.fhwa.dot.gov/bridge/prefab/if09010/appd.cfm)

Figure 7 Examples of HP sections pile bents.

In a pile-bent, the extended H-pile functions as a structural member under combined axial and lateral loads where lateral buckling and lateral deformation of the pile define the stability of the pile. Axial resistance of the partially embedded H-pile follows the same design procedure as for fully embedded H-pile (See Section 1.3). The following sections focus on the lateral resistance of H-piles, briefly introducing available analysis methodologies and important design parameters.

4.1.2 Analysis methods

Various methods have been adopted for determining the moment, lateral deformation, and critical lateral buckling load of extended piles or partially embedded piles. Methods investigate the effects of different parameters, such as soil-pile interface, soil stiffness, pile stiffness and geometric properties, and lateral deformation on the performance of the extended pile. Approaches to extended pile analysis include empirical methods, analytical methods, finite element methods, load-transfer or P-y curve methods, boundary element method (BEM), virtual work, reliability analysis, and cyclic lateral loading. These methods can be applied either separately or combined for modeling the soil-pile system and predict the performance of the pile accurately. The assumption as to whether the soil behaves either linearly elastic or elastic-perfectly-plastic governs the selection of a proper analysis method for evaluating the lateral performance of the pile.

AASHTO/LRFD §10.7.3.12 recommends the use of P-y curves, developed for the soils at a site, for evaluating the lateral resistance of piles under horizontal loading. Emphasis has been put on the appropriate selection of top boundary condition of the pile since it will affect the moment distribution along the pile length (Refer to Figure 8). In addition, the P-y curves should

be modified using factors given in AASHTO/LRFD Table 10.7.2.4-1 in order to account for group effects of a pile group.

Bodkowska et al. (1996) investigated the variation of critical buckling load of partially embedded piles considering the effects of different design parameters such as pile stiffness, subgrade modulus, and pile toe location change. They developed a relationship predicting the variation of critical buckling load with respect to the parameters related of the soil-pile system using the principles of virtual work and performing a first-order sensitivity analysis. The soil was modeled based on a Winkler-type elastic foundation. Design parameters were pile cross-section type and material properties, soil properties, and pile end boundary conditions. The authors ignored the effects of skin friction in the analysis basing on the result of Reddy and Valsanger (1970) showing that if the ratio of the embedded part of the pile to its total length is less than 60% then the skin friction effect is negligible.

Fatahi et al. (2014) conducted research on the performance of fixed-head piles embedded into soft clay and medium dense sand under lateral loads considering the effects of parameters related to soil and soil interface. Initially the soil-pile system under lateral load was modeled using the boundary element method (BEM) to investigate the effects of soil stiffness on pile head displacement and the soil reaction. The pile was assumed to behave elastically in an isotropic, semi-infinite and elastic-perfectly-plastic soil. BEM is a simple method and cannot estimate the interaction between soil and pile under lateral loadings in multilayered soil systems. In addition, the effect of shear stresses along the soil-pile interface was excluded from the BEM model in order to reduce complexity. To accurately investigate the performance of the laterally loaded pile and account for the complex behavior of soil-pile interface, the three-dimensional finite element model (FEM) was developed. The soil-pile interface reduction factor and the coefficient of

lateral earth pressure were incorporated into the FEM model to perfectly examine the soil-pile behavior. The results of the theoretical analysis were confirmed with the data from field measurements.

It is worth noting that application of computer-aided programs have also been indicated in the literature since manual analysis of nonlinear soil-pile interaction is cumbersome and time consuming. The programs are typically based on the principles of analytical methods introduced previously and are capable of processing a large amount of data, performing nonlinear analyses with great precision, and providing desired outputs. The desired outputs from these programs are moment-curvature diagrams, moment interaction diagrams, and the P-y curves.

4.1.3 Effective length (L_e)

Effective length of a partially embedded pile is the equivalent unbraced length of the real pile and is used to facilitate the calculation of lateral capacity of the pile. AASHTO/LRFD §10.7.3.13.4 defines effective length L_e as the laterally unsupported length of the extended pile plus an embedded length or depth of fixity L_f. Depth of fixity is taken to where the moment is zero along the embedded portion of the pile as shown in Figure 9. Davisson and Robinson's model for estimating the depth of fixity uses the equivalent elastic model of the soil-pile system to approximate the complex nonlinear interaction of the soil-pile system. The piles are considered fully fixed at some depth below ground surface and the soil is ignored. The boundary condition for the head of the pile must be specified as either free (shown in Figure 9) or fixed.

L_f may be taken as:

- For clay: $L_f = 1.4[E_p I_w / E_s]^{0.25}$
- For sand: $L_f = 1.8[E_p I_w / n_h]^{0.2}$

Where E_p = modulus of elasticity of pile (ksi); I_w = weak axis moment of inertia for pile (ft^4); E_s = soil modulus for clays = 0.465 S_u (ksi); S_u = undrained shear strength of clays (ksf); and n_h = rate of increase of soil modulus with depth for sands as specified in AASHTO/LRFD Table C10.4.6.3-2 repeated here as Table 21.

Table 21 Rate of increase of soil modulus with depth n_h (ksi/ft) for sand

Consistency	Dry or Moist	Submerged
Loose	0.417	0.208
Medium	1.11	0.556
Dense	2.78	1.39

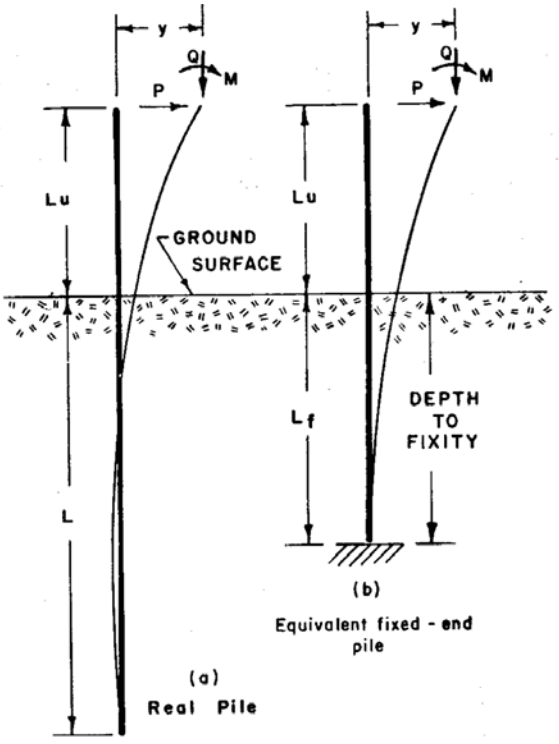

Figure 8 Equivalent model of fixed-head pile by Wilson et al. 1963.

Robinson et al. (2006) explained possible drawbacks of Davisson and Robinson's model for computing L_f. For multiple soil layer profile it is required to define an equivalent layer of either clay or sand in order to use the equations. Additionally, the model doesn't distinguish between free-headed and fix-headed piles and it cannot be used to assess lateral displacements. In addition, the equivalent model for the fixed-head condition results larger moments compared to the free-head condition (Wilson & Hilts, 1963).

On the other hand, Robinson et al. (2006) proposes an equivalent elastic model for defining depth of fixity for an extended pile with either free- or fixed-head boundary conditions. This equivalent elastic model is based on the results of nonlinear lateral single-pile analyses. The equivalent elastic model defines some parameters such that the pile with estimated effective length, L_e, would respond the same as a pile embedded in soil with nonlinear behavior. Figure 10 shows the proposed model for both free- and fixed-head boundary conditions.

Parameter	**Free-head condition**	**Fixed-head condition**
Effective length L_e	$L_e = M_{max}/V$	$L_e = 2M_{max}/V$
Inertia reduction factor α	$\alpha = L_e^3 V/3E_pI_p\Delta_t$	$\alpha = L_e^3 V/12E_pI_p\Delta_t$
Effective length factor k	$k = L_b/L_e$	$k = L_b/L_e$
Axial deformation factor β	$\beta = P\ L_e/\Delta_z E_p A_p$	$\beta = P\ L_e/\Delta_z E_p A_p$

Where, M_{max} = maximum moment developed in both the equivalent model and the nonlinear soil-pile model; V = lateral force applied at the top of the pile in both the equivalent model and the nonlinear soil-pile model; E_p = elastic modulus of the pile material; I_p = moment of inertia of the pile about the axis perpendicular to the applied load (I_p in the equivalent model will give the same lateral stiffness as the nonlinear soil-pile model); Δ_t = displacement at the top

of the pile caused by the application of the lateral load V; L_b = effective length for a stability (buckling) check of the pile, and β = factor that is applied to the area of the pile in the equivalent model to result in the same axial deformation as the nonlinear soil-pile model under the effect of the axial load P.

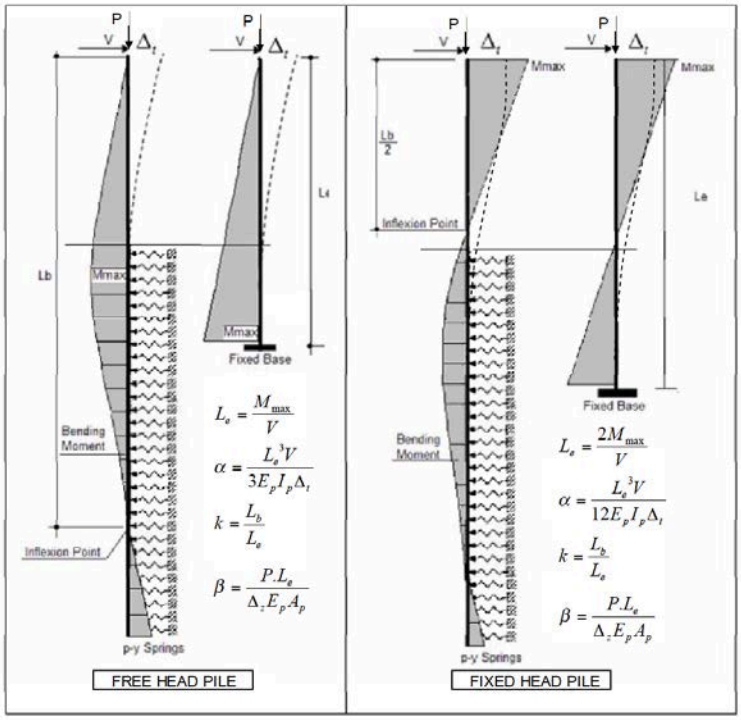

Figure 9 Equivalent elastic model by Robinson et al. 2006.

Parameters like effective length of the pile, L_e, inertia reduction factor, α, and effective length factor, k, in the equivalent method are sensitive to the level of axial and lateral loading applied to a nonlinear single-pile model. Sensitivity analysis shows that with an increase of lateral load, the stiffness of the soil-pile system degrades. With an increase of lateral load, L_e tends to increase while α decreases; the k-factor doesn't change with an increase of lateral load

magnitude. The axial load affects the response of the system by inducing second order moments that increases the lateral deflection (Robinson et al. 2006).

In order to have reliable results for a nonlinear soil-pile system from the analysis of an equivalent model the level of applied load has to be selected carefully. An equivalent model based on equivalent parameters estimated using higher loading values will deflect more, develop higher moments, and predict a lower axial capacity. Thus it will be conservative for design purposes (Robinson et al. 2006).

Lastly, Shama et al. (2002) took a different approach toward determination of L_f for a pile with an extended length h, embedded into a concrete cap beam at the top (See Figure 10). The effective length is defined as the clear distance between the inflection point and the pile-cap connection. A theoretical equation is derived based on principles of virtual work for determining depth of fixity, denoted Z, from ground surface to the plastic hinge in the portion of pile within the soil. The idealized model assumed the lateral soil reaction to be zero at a depth of $1.5d_p$ and equal to $9.0C_ud_p$ below this depth, where C_u is defined as the cohesion of the soil considered, determined from undrainded triaxial, direct shear or vane tests, and d_p is the depth of the steel pile section. Applying the theory of virtual work, Z is defined as follows in cohesive soils:

$$Z = (h + e)\left[\sqrt{1 + \frac{0.44M_p}{C_u d_p (h + e)^2}} - 1\right] + e$$

Where, h = the clear distance from the plastic hinge at pile-to-pile cap connection to the soil surface, e = soil depth where the lateral soil reaction equals zero, and M_p = moment at the plastic hinge.

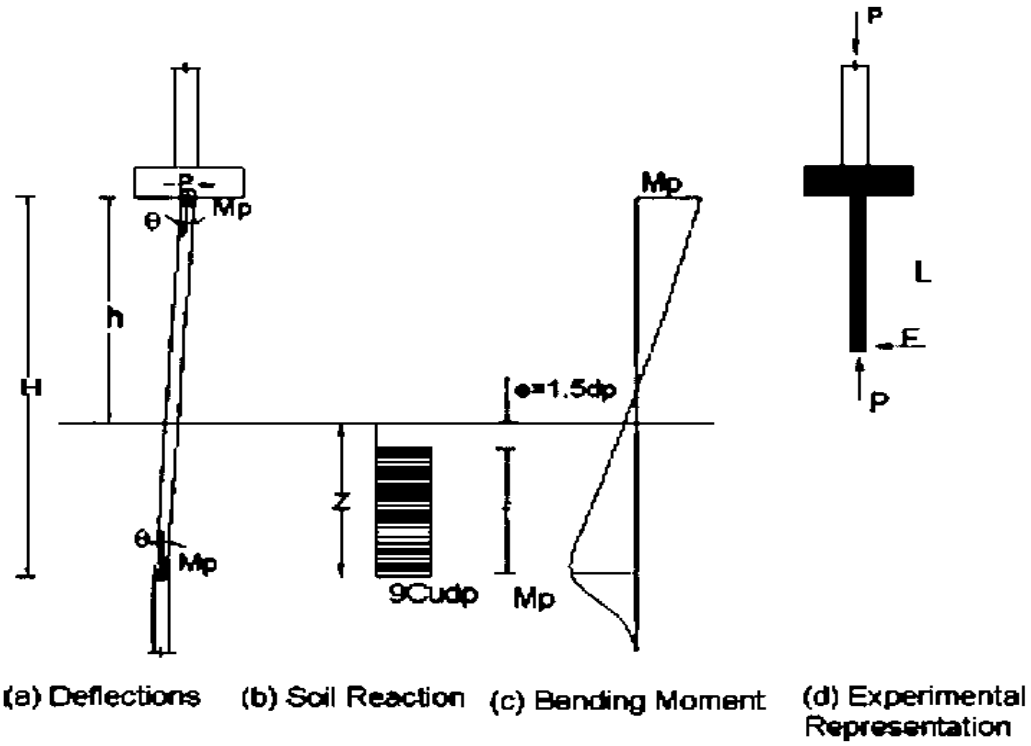

Figure 10 Equivalent model for a fixed-head extended pile by Shama et al. 2002.

4.1.4 Pile-to-pile cap connection fixity

Fixity of the pile-cap connection defines the load-deflection response of the pile or pile group and determines the magnitude and location of the maximum moment at the connection. The fixity of the pile-cap connection is usually assumed to vary between fully fixed and [50 percent] partially fixed. The degree of pile-cap connection fixity is often determined empirically. Key factors that must be considered in determining or estimating fixity at the pile-cap connection including: (NHI-Course-No.132068, 2001)

i. Depth of pile embedment into the cap where empirically it is proved that an embedment depth of 2D to 3D into the cap provides full fixity under service loads (D = pile diameter or depth).

ii. Magnitude of bending moment at pile-cap connection

iii. Pile type and geometry

iv. Pile-to-pile cap connection detail

4.1.5 Failure modes of pile under lateral loads

Depending on the boundary condition of the pile at the top, three modes of failure have been recognized for piles under combined axial and lateral loads. The pile is assumed to be fixed at the end embedded into the soil. For the free-head condition, failure may occur either by a lateral bearing failure of the soil or by formation of a plastic hinge at the embedded portion of the pile. For the fixed-head condition, an additional failure mode occur at the pile-cap connection where a second plastic hinge is formed, see Figure 11 (Fatahi et al. 2014)

The dominance of a specific failure mode depends on the stiffness of the soil, stiffness and strength of the pile, length of the pile, and intensity of the lateral load. For instance, in piles having a shorter length the failure occurs due to lateral yielding of surrounding soil and are therefore largely unaffected by pile yield strength. In longer piles, however, the failure occurs by yielding of the pile material itself prior to soil failure. A pile having a greater capacity due to a larger yield capacity may have the effect of 'shifting' the failure back to soil for a given pile length. For better results it is suggested that the horizontal capacity of a pile should be determined considering all failure modes and selecting the lower lateral load capacity calculated based on all failure modes (Fatahi et al. 2014)

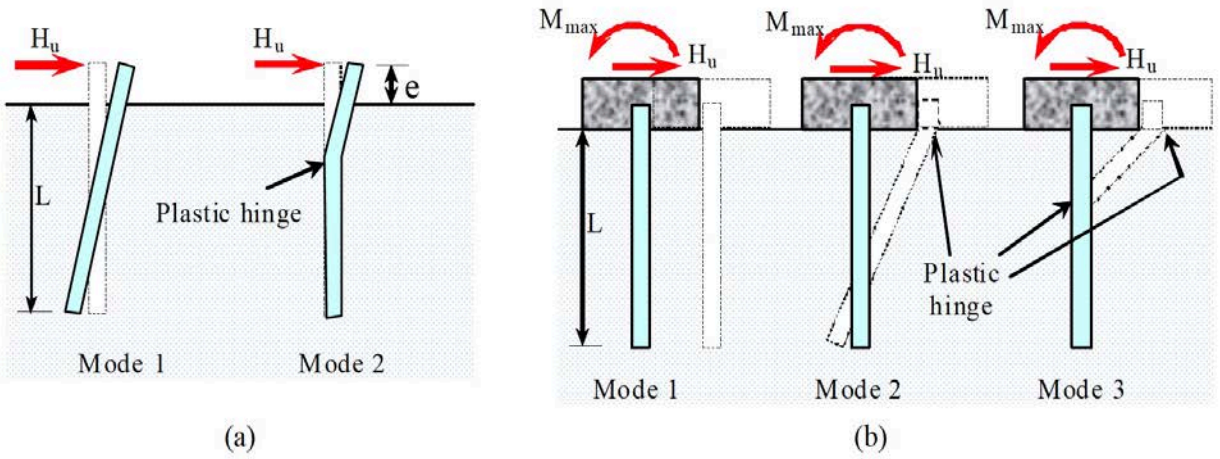

Figure 11 Failure modes for (a) free-head & (b) fixed-head boundary conditions (Fatahi et al., 2014)

Lateral capacity doesn't represent a realistic basis for the design of laterally loaded piles because mobilization of ultimate lateral capacity of the soil requires large lateral displacements. As mentioned earlier, the lateral capacity of a pile under lateral load is governed by the lateral deflection of the pile. This deflection must not exceed the tolerable lateral movement specified for the foundation. The lateral deflection of an extended pile is typically the passive failure of the soil. But the occurrence of this potential soil failure is conditioned with the occurrence of relatively large deflections of the pile that generally exceed tolerable movements. For this reason the design of piles subjected to lateral loads is commonly based on structural capacity and load-deflection behavior considerations rather than on lateral bearing failure of the pile (NHI-Course-No.132068, 2001).

For piles subjected to both axial and lateral loading, the structural resistance of the pile as a beam-column must be checked using the conventional interaction equations (AASHTO/LRFD §6.9.2.2, identical to equations H1-1a and H1-1b of AISC (2005)):

If $P_u/P_r < 0.2$, then

$$P_u/(2P_r) + (M_{ux}/M_{rx} + M_{uy}/M_{ry}) \leq 1.0$$

If $Pu/P_r \geq 0.2$, then

$$P_u/P_r + 8/9\ (M_{ux}/M_{rx} + M_{uy}/M_{ry}) \leq 1.0$$

Where, M_{rx} = factored flexural resistance about the x-axis (kip-in), M_{ry} = factored flexural resistance about the y-axis (kip-in), and $M_{ux,}$ M_{uy} = factored flexural moment about the x-and y-axis determined from second-order elastic analysis which will count for the moment magnification caused by factored axial load (kip-in). The interaction equations represent an iterative method where structural capacity of the pile is checked against applied lateral and axial loads.

Finally, axial and lateral ground displacement can be determined by conventional methods using empirical correlations with in-situ test results or measurements by in-situ or laboratory test methods to estimate engineering soil properties. Computer programs, based on t-z and p-y curve methods, are available to compute the axial and lateral deflection of piles. Often the tolerable axial and lateral movement of driven piles are set considering the either criteria developed for the superstructure or the effects of foundation movement on adjacent structures.

4.1.6 Summary

It should be clear from the foregoing discussion of extended or partially embedded piles, that pile material capacity has a minimal effect on pile or pile group behavior. Deflections ‘control’ design and are primarily a function of soil properties and pile stiffness, which is unaffected by yield strength. The same potential issues raised for braced piles (Section 1.2) affect extended piles.

5.0 CONCLUSIONS

This research investigates the capacity and drivability of 50 ksi H-piles. Driven H-piles have wide application in deep foundations and are meant to support the structure on deeper and stronger layers of ground in the case of weaker subsurface ground materials. Preferred material specification for H-pile shapes is ASTM A572 (2013) Grade 50 High Strength-Low Alloy Steel. However, there are some issues associated with 50 ksi H-piles due to their higher strength compared to 36 ksi – the yield capacity for which most design provisions were established. Higher design strength results smaller sections, which will adversely affect pile capacity. As the yield strength increases from 36 to 50 ksi, the flange and web slenderness ratios defining compact and noncompact section limits – both a function of $\sqrt{E/F_y}$ – fall 18%. However, resulting decreases in capacity over the compact shape calculation is at worst 3.6% for axial and 8% for flexure for the most slender shape. Section loss due to effect of corrosion (1/16 in) is more critical for the smaller pile sizes that may be permitted by utilizing the higher yield strength.

A comprehensive parametric study, on the soil-pile-hammer system for a driven H-pile consisting of 126 base scenarios (i.e.: 3 pile shapes x 3 pile lengths x 2 shaft friction values x 7 analysis cases) was carried out. Additional sensitivity analyses addressing toe damping, toe quake and skin damping were also made on a subset of scenarios. The following conclusions regarding the capacity and drivability of 50 ksi H-piles were drawn:

I. The driving stress will always exceed the ultimate stress. Therefore piles cannot achieve an ultimate stress of A_sF_y when driving stress is limited to $0.9A_sF_y$. However, this does not imply that a design capacity of $0.5A_sF_y$ cannot be achieved, it only requires PDA to accompany driving – in which case the target ultimate capacity is only $0.5A_sF_y/0.65 = 0.77A_sF_y$ rather than $0.5A_sF_y/0.50 = A_sF_y$ when no PDA is used. By the same token, the minimum permissible driving stress of 25 ksi = $0.5A_sF_y$ implies that the minimum drivable ultimate capacity is only somewhat lower than this.

II. Driving piles to the maximum permitted driving stress of $0.90A_sF_y$ = 45 ksi, resulted in pile capacities ranging from $0.64A_sF_y$ to $0.76A_sF_y$.

III. For driving heavier pile sections larger hammers are required since driving stress increases with pile sections.

IV. For a given pile section, driving stress decreases with increased pile length.

V. The driving stress also decreases when shaft friction is increased from 0.20 to 0.30. This effect is clearly more pronounced for longer piles and is somewhat more pronounced for larger pile sections due to their greater perimeter dimension.

VI. All HP10x57 and HP12x74 piles had available hammer strokes exceeding the recommended limit of 0.5 ft. The available range decreased with increasing pile size. Only HP14x117 piles having shaft friction = 0.30 exhibited hammer stroke ranges exceeding 0.5 ft.

VII. The theoretical increase in pile capacity realized by accounting for the increase of F_y from 36 to 50 ksi and the revisions to the PennDOT standard is a factor of 1.31. (i.e.: from (0.35 x 36 ksi)A_s to (0.50 x 0.66 x 50 ksi)A_s) This theoretical increase is achievable for all cases considered.

APPENDIX A

MASTER DATA

Table 1A Master data – Base analyses

ID		HP	As	Stress at refusal	Capacity at refusal	Length	Friction	Toe Damping	Toe Quake	Skin Damping	Smallest Hammer	Driving stress at refusal	Cal. stroke	Energy
BASE			in^2	$1/A_sFy$	kips	ft	%					ksi	ft	k-ft
1	1a	10x57	16.8	1.00	840	20	0.20	0.10	0.05	0.05	ICE I-30v2	66	8.86	23.80
2	1b	10x57	16.8	0.66	554	20	0.20	0.10	0.05	0.05	ICE I-12v2	42	9.05	11.40
3	1c	10x57	16.8	0.50	420	20	0.20	0.10	0.05	0.05	ICE I-12v2	30	6.70	7.20
4	2a	10x57	16.8	0.70	588	20	0.20	0.10	0.05	0.05	ICE I-30v2	45	5.95	12.4
5	2b	10x57	16.8	0.70	591	20	0.20	0.10	0.05	0.05	ICE I-12v2	45	10.00	13.00
6	3	10x57	16.8	0.66	554	20	0.20	0.10	0.05	0.05	ICE I-30v2	43	5.59	11.10
7	4	10x57	16.8	0.45	375	20	0.20	0.10	0.05	0.05	ICE I-30v2	25	4.20	5.70
8	1a	10x57	16.8	1.00	840	20	0.30	0.10	0.05	0.05	ICE I-30v2	64	8.93	24.10

Table 1A (continued)

9	1b	10x57	16.8	0.66	554	20	0.30	0.10	0.05	0.05	ICE I-12v2	40	9.10	11.60
10	1c	10x57	16.8	0.50	420	20	0.30	0.10	0.05	0.05	ICE I-12v2	29	6.70	7.20
11	2a	10x57	16.8	0.70	588	20	0.30	0.10	0.05	0.05	ICE I-30v2	45	5.95	11.80
12	2b	10x57	16.8	0.71	600	20	0.30	0.10	0.05	0.05	ICE I-12v2	45	10.30	13.80
13	3	10x57	16.8	0.66	554	20	0.30	0.10	0.05	0.05	ICE I-30v2	41	5.60	11.10
14	4	10x57	16.8	0.44	372	20	0.30	0.10	0.05	0.05	ICE I-30v2	25	4.20	5.70
15	1a	10x57	16.8	1.00	840	50	0.20	0.10	0.05	0.05	ICE I-30v2	59.7	11.40	42.90
16	1b	10x57	16.8	0.66	554	50	0.20	0.10	0.05	0.05	PilcoD1942	38.0	8.30	18.80
17	1c	10x57	16.8	0.50	420	50	0.20	0.10	0.05	0.05	ICE I-12v2	29.1	7.40	10.60
18	2a	10x57	16.8	0.74	618	50	0.20	0.10	0.05	0.05	ICE I-30v2	45.0	7.90	25.10
19	2b	10x57	16.8	0.75	627	50	0.20	0.10	0.05	0.05	PilcoD1942	44.6	10.10	25.00
20	3	10x57	16.8	0.66	554	50	0.20	0.10	0.05	0.05	ICE I-30v2	39.2	6.70	19.20
21	4	10x57	16.8	0.43	363	50	0.20	0.10	0.05	0.05	ICE I-30v2	24.7	4.50	8.50
22	1a	10x57	16.8	1.00	840	50	0.30	0.10	0.05	0.05	ICE I-36v2	60.3	9.77	43.50
23	1b	10x57	16.8	0.66	554	50	0.30	0.10	0.05	0.05	PilcoD1942	36.5	8.40	19.50
24	1c	10x57	16.8	0.50	420	50	0.30	0.10	0.05	0.05	ICE I-12v2	26.3	7.51	10.80
25	2a	10x57	16.8	0.76	642	50	0.30	0.10	0.05	0.05	ICE I-36v2	45.0	7.15	26.70
26	2b	10x57	16.8	0.76	635	50	0.30	0.10	0.05	0.05	PilcoD1942	43.4	10.50	26.60
27	3	10x57	16.8	0.66	554	50	0.30	0.10	0.05	0.05	ICE I-36v2	37.6	6.025	19.10
28	4	10x57	16.8	0.46	388	50	0.30	0.10	0.05	0.05	ICE I-36v2	25	4.50	9.60
29	1a	10x57	16.8	1.00	840	80	0.20	0.10	0.05	0.05	ICE I-36v2	59.2	10.70	58.00
30	1b	10x57	16.8	0.66	554	80	0.20	0.10	0.05	0.05	PilcoD1942	37.0	8.50	22.90
31	1c	10x57	16.8	0.50	420	80	0.20	0.10	0.05	0.05	ICE I-12v2	29.0	7.50	12.00
32	2a	10x57	16.8	0.80	672	80	0.20	0.10	0.05	0.05	ICE I-36v2	46.2	8.01	37.00
33	2b	10x57	16.8	0.75	632	80	0.20	0.10	0.05	0.05	PilcoD1942	43.3	10.60	31.20
34	3	10x57	16.8	0.66	554	80	0.20	0.10	0.05	0.05	ICE I-36v2	37.3	6.41	25.70
35	4	10x57	16.8	0.46	389	80	0.20	0.10	0.05	0.05	ICE I-36v2	24.8	4.68	13.10
36	1a	10x57	16.8	1.00	840	80	0.30	0.10	0.05	0.05	ICE I-36v2	56.6	11.05	61.30
37	1b	10x57	16.8	0.66	554	80	0.30	0.10	0.05	0.05	PilcoD1942	32.9	8.65	23.60
38	1c	10x57	16.8	0.50	420	80	0.30	0.10	0.05	0.05	ICE I-12v2	26.0	7.64	12.20
39	2a	10x57	16.8	0.80	674	80	0.30	0.10	0.05	0.05	ICE I-36v2	45.0	8.25	39.90
40	2b	10x57	16.8	0.74	619	80	0.30	0.10	0.05	0.05	PilcoD1942	37.8	10.60	31.50
41	3	10x57	16.8	0.66	554	80	0.30	0.10	0.05	0.05	ICE I-36v2	35.4	6.49	26.70

Table 1A (continued)

42	4	10x57	16.8	0.49	415	80	0.30	0.10	0.05	0.05	ICE I-36v2	26	5.00	16.00
43	1a	12x74	21.8	1.00	1090	20	0.20	0.10	0.05	0.05	ICE I-30v2	65	10.95	30.80
44	1b	12x74	21.8	0.66	719	20	0.20	0.10	0.05	0.05	ICE I-30v2	42	6.68	14.70
45	1c	12x74	21.8	0.50	545	20	0.20	0.10	0.05	0.05	ICE I-12v2	31	8.20	9.50
46	2a	12x74	21.8	0.70	767	20	0.20	0.10	0.05	0.05	ICE I-30v2	45	7.20	16.60
47	2b	12x74	21.8	0.70	767	20	0.20	0.10	0.05	0.05	ICE I-30v2	45	7.20	16.60
48	3	12x74	21.8	0.66	719	20	0.20	0.10	0.05	0.05	ICE I-30v2	42	6.68	14.70
49	4	12x74	21.8	0.42	456	20	0.20	0.10	0.05	0.05	ICE I-30v2	25	4.60	7.10
50	1a	12x74	21.8	1.00	1090	20	0.30	0.10	0.05	0.05	ICE I-30v2	63	11.05	31.50
51	1b	12x74	21.8	0.66	719	20	0.30	0.10	0.05	0.05	ICE I-30v2	41	6.71	15.00
52	1c	12x74	21.8	0.50	545	20	0.30	0.10	0.05	0.05	ICE I-12v2	28	8.27	9.70
53	2a	12x74	21.8	0.72	784	20	0.30	0.10	0.05	0.05	ICE I-30v2	45	7.50	17.90
54	2b	12x74	21.8	0.72	784	20	0.30	0.10	0.05	0.05	ICE I-30v2	45	7.50	17.90
55	3	12x74	21.8	0.66	719	20	0.30	0.10	0.05	0.05	ICE I-30v2	41	6.70	14.90
56	4	12x74	21.8	0.45	486	20	0.30	0.10	0.05	0.05	ICE I-30v2	26	4.80	7.90
57	1a	12x74	21.8	1.00	1090	50	0.20	0.10	0.05	0.05	ICE I-36v2	62	11.81	52.00
58	1b	12x74	21.8	0.66	719	50	0.20	0.10	0.05	0.05	PilcoD1942	39	9.75	23.60
59	1c	12x74	21.8	0.50	545	50	0.20	0.10	0.05	0.05	ICE I-12v2	31	8.66	12.90
60	2a	12x74	21.8	0.73	800	50	0.20	0.10	0.05	0.05	ICE I-36v2	45	8.20	29.90
61	2b	12x74	21.8	0.70	763	50	0.20	0.10	0.05	0.05	PilcoD1942	42	10.60	26.50
62	3	12x74	21.8	0.66	719	50	0.20	0.10	0.05	0.05	ICE I-36v2	39	7.11	23.40
63	4	12x74	21.8	0.43	466	50	0.20	0.10	0.05	0.05	ICE I-36v2	25	4.90	11.30
64	1a	12x74	21.8	1	1090	50	0.30	0.1	0.05	0.05	ICE I-46v2	61.43	10.27	54.9
65	1b	12x74	21.8	0.66	719	50	0.30	0.10	0.05	0.05	PilcoD1942	35	9.85	24.10
66	1c	12x74	21.8	0.50	545	50	0.30	0.10	0.05	0.05	ICE I-12v2	28	8.78	13.10
67	2a	12x74	21.8	0.75	816	50	0.30	0.10	0.05	0.05	ICE I-46v2	45	7.40	33.30
68	2b	12x74	21.8	0.69	751	50	0.30	0.10	0.05	0.05	PilcoD1942	37	10.60	26.60
69	3	12x74	21.8	0.66	719	50	0.30	0.10	0.05	0.05	ICE I-46v2	38	6.30	24.70
70	4	12x74	21.8	0.45	488	50	0.30	0.10	0.05	0.05	ICE I-46v2	25	4.60	12.30
71	1a	12x74	21.8	1	1090	80	0.20	0.1	0.05	0.05	ICE I-46v2	60.7	11.24	73
72	1b	12x74	21.8	0.66	719	80	0.20	0.10	0.05	0.05	PilcoD1942	39	9.80	26.70
73	1c	12x74	21.8	0.50	545	80	0.20	0.10	0.05	0.05	ICE I-12v2	31	8.75	14.00
74	2a	12x74	21.8	0.80	872	80	0.20	0.10	0.05	0.05	ICE I-46v2	45	8.40	47.60

Table 1A (continued)

75	2b	12x74	21.8	0.69	756	80	0.20	0.10	0.05	0.05	PilcoD1942	41	10.60	29.70
76	3	12x74	21.8	0.66	719	80	0.20	0.10	0.05	0.05	ICE I-46v2	37	6.70	33.00
77	4	12x74	21.8	0.46	503	80	0.20	0.10	0.05	0.05	ICE I-46v2	25	4.80	16.30
78	1a	12x74	21.8	1.00	1090	80	0.30	0.10	0.05	0.05	ICE I-46v2	55	11.61	77.50
79	1b	12x74	21.8	0.66	719	80	0.30	0.10	0.05	0.05	PilcoD1942	35	10.03	27.50
80	1c	12x74	21.8	0.50	545	80	0.30	0.10	0.05	0.05	ICE I-12v2	28	8.92	14.30
81	2a	12x74	21.8	0.89	972	80	0.30	0.10	0.05	0.05	ICE I-46v2	45	9.00	54.10
82	2b	12x74	21.8	0.67	733	80	0.30	0.10	0.05	0.05	PilcoD1942	36	10.60	29.60
83	3	12x74	21.8	0.66	719	80	0.30	0.10	0.05	0.05	ICE I-46v2	34	6.79	34.00
84	4	12x74	21.8	0.50	541	80	0.30	0.10	0.05	0.05	ICE I-46v2	25	5.20	20.00
85	1a	14x117	34.4	1.00	1720	20	0.20	0.10	0.05	0.05	ICE I-46v2	66	11.45	47.60
86	1b	14x117	34.4	0.66	1135	20	0.20	0.10	0.05	0.05	ICE I-30v2	46	9.75	25.40
87	1c	14x117	34.4	0.50	860	20	0.20	0.10	0.05	0.05	PilcoD1942	32	8.55	15.40
88	2a	14x117	34.4	0.70	1204	20	0.20	0.10	0.05	0.05	ICE I-46v2	45	7.46	24.90
89	2b	14x117	34.4	0.64	1106	20	0.20	0.10	0.05	0.05	ICE I-30v2	45	9.50	24.60
90	3	14x117	34.4	0.66	1135	20	0.20	0.10	0.05	0.05	ICE I-46v2	42	7.03	22.60
91	4	14x117	34.4	0.41	699	20	0.20	0.10	0.05	0.05	ICE I-46v2	25	5.00	10.50
92	1a	14x117	34.4	1.00	1720	20	0.30	0.10	0.05	0.05	ICE I-46v2	64	11.60	48.70
93	1b	14x117	34.4	0.66	1135	20	0.30	0.10	0.05	0.05	ICE I-30v2	42	9.81	25.70
94	1c	14x117	34.4	0.50	860	20	0.30	0.10	0.05	0.05	PilcoD1942	30	8.59	15.50
95	2a	14x117	34.4	0.70	1204	20	0.30	0.10	0.05	0.05	ICE I-46v2	45	7.54	25.60
96	2b	14x117	34.4	0.70	1204	20	0.30	0.10	0.05	0.05	ICE I-30v2	45	10.58	28.60
97	3	14x117	34.4	0.66	1135	20	0.30	0.10	0.05	0.05	ICE I-46v2	41	7.10	23.10
98	4	14x117	34.4	0.44	760	20	0.30	0.10	0.05	0.05	ICE I-46v2	25	5.10	12.30
99	1a	14x117	34.4	0.84	1444	50	0.20	0.10	0.05	0.05	ICE I-46v2	52	11.81	62.20
100	1b	14x117	34.4	0.66	1135	50	0.20	0.10	0.05	0.05	ICE I-30v2	45	10.30	33.70
101	1c	14x117	34.4	0.50	860	50	0.20	0.10	0.05	0.05	PilcoD1942	32	8.81	19.30
102	2a	14x117	34.4	0.72	1236	50	0.20	0.10	0.05	0.05	ICE I-46v2	45	9.60	46.40
103	2b	14x117	34.4	0.66	1135	50	0.20	0.10	0.05	0.05	ICE I-30v2	45	10.30	33.70
104	3	14x117	34.4	0.66	1135	50	0.20	0.10	0.05	0.05	ICE I-46v2	41	8.48	38.60
105	4	14x117	34.4	0.41	701	50	0.20	0.10	0.05	0.05	ICE I-46v2	25	5.20	15.90
106	1a	14x117	34.4	0.83	1420	50	0.30	0.10	0.05	0.05	ICE I-46v2	46	11.81	62.30
107	1b	14x117	34.4	0.66	1135	50	0.30	0.10	0.05	0.05	ICE I-30v2	41	10.50	34.60

Table 1A (continued)

108	1c	14x117	34.4	0.50	860	50	0.30	0.10	0.05	0.05	PilcoD1942	29	8.95	19.70
109	2a	14x117	34.4	0.81	1394	50	0.30	0.10	0.05	0.05	ICE I-46v2	45	11.40	59.40
110	2b	14x117	34.4	0.72	1232	50	0.30	0.10	0.05	0.05	ICE I-30v2	45	12.00	41.50
111	3	14x117	34.4	0.66	1135	50	0.30	0.10	0.05	0.05	ICE I-46v2	37	8.58	39.20
112	4	14x117	34.4	0.46	795	50	0.30	0.10	0.05	0.05	ICE I-46v2	25	5.80	20.00
113	1a	14x117	34.4	0.82	1407	80	0.20	0.10	0.05	0.05	ICE I-46v2	51	11.81	72.90
114	1b	14x117	34.4	0.66	1135	80	0.20	0.10	0.05	0.05	ICE I-30v2	45	10.54	38.70
115	1c	14x117	34.4	0.50	860	80	0.20	0.10	0.05	0.05	PilcoD1942	31	8.91	20.60
116	2a	14x117	34.4	0.72	1244	80	0.20	0.10	0.05	0.05	ICE I-46v2	45	10.00	57.60
117	2b	14x117	34.4	0.66	1135	80	0.20	0.10	0.05	0.05	ICE I-30v2	45	10.54	38.70
118	3	14x117	34.4	0.66	1135	80	0.20	0.10	0.05	0.05	ICE I-46v2	41	8.68	46.20
119	4	14x117	34.4	0.42	718	80	0.20	0.10	0.05	0.05	ICE I-46v2	25	5.40	19.50
120	1a	14x117	34.4	0.81	1389	80	0.30	0.10	0.05	0.05	ICE I-46v2	45	11.81	72.80
121	1b	14x117	34.4	0.66	1135	80	0.30	0.10	0.05	0.05	ICE I-30v2	40	10.81	39.70
122	1c	14x117	34.4	0.50	860	80	0.30	0.10	0.05	0.05	PilcoD1942	28	9.10	21.10
123	2a	14x117	34.4	0.81	1389	80	0.30	0.10	0.05	0.05	ICE I-46v2	45	11.81	72.80
124	2b	14x117	34.4	0.68	1178	80	0.30	0.10	0.05	0.05	ICE I-30v2	42	11.50	43.60
125	3	14x117	34.4	0.66	1135	80	0.30	0.10	0.05	0.05	ICE I-46v2	36	8.84	47.30
126	4	14x117	34.4	0.46	795	80	0.30	0.10	0.05	0.05	ICE I-46v2	25	5.93	23.80

Table 2A Sensitivity analyses results

ID	HP	As	Stress at refusal	Capacity at refusal	Length	Friction	Toe Damping	Toe Quake	Skin Damping	Smallest Hammer	Driving stress at refusal	Cal. stroke	Energy
SENSITIVITY		in^2	$1/A_sFy$	kips	ft	%					ksi	ft	k-ft
127	12x74	21.8	0.97	1056	50	0.20	0.10	0.05	0.20	ICE I-46v2	58	11.81	67.90
128	12x74	21.8	0.66	719	50	0.20	0.10	0.05	0.20	ICE I-30v2	39	9.00	29.60
129	12x74	21.8	0.50	545	50	0.20	0.10	0.05	0.20	ICE I-12v2	30	10.07	15.90
130	12x74	21.8	0.76	831	50	0.20	0.10	0.05	0.20	ICE I-46v2	45	8.49	41.70
131	12x74	21.8	0.44	480	50	0.20	0.10	0.05	0.20	ICE I-46v2	25	4.90	14.90
132	12x74	21.8	1.00	1090	50	0.20	0.15	0.10	0.05	ICE I-46v2	65	11.34	65.30
133	12x74	21.8	0.66	719	50	0.20	0.15	0.10	0.05	ICE I-30v2	45	8.92	29.70
134	12x74	21.8	0.50	545	50	0.20	0.15	0.10	0.05	ICE I-12v2	33	10.30	16.90
135	12x74	21.8	0.70	764	50	0.20	0.15	0.10	0.05	ICE I-46v2	45	7.37	34.00
136	12x74	21.8	0.43	469	50	0.20	0.15	0.10	0.05	ICE I-46v2	25	4.69	13.30
137	12x74	21.8	0.92	1000	50	0.20	0.15	0.10	0.20	ICE I-46v2	55	11.81	69.10
138	12x74	21.8	0.66	719	50	0.20	0.15	0.10	0.20	ICE I-30v2	40	10.25	36.70
139	12x74	21.8	0.50	545	50	0.20	0.15	0.10	0.20	PilcoD1942	30	8.84	21.10
140	12x74	21.8	0.79	864	50	0.20	0.15	0.10	0.20	ICE I-46v2	45	9.40	49.70
141	12x74	21.8	0.43	468	50	0.20	0.15	0.10	0.20	ICE I-46v2	25	4.88	14.60

BIBLIOGRAPHY

AASHTO. (2014). *Bridge Design Specifications* (7th ed.). Washington DC, District of Columbia, United States of America: American Association of State Highway and Transportation Officials.

AASHTO. (2010). Bridge Design Specifications (5th ed.). Washington DC, District of Columbia, United States of America: American Association of State Highway and Transportation Officials.

AASHTO. (2007). Bridge Design Specifications (4th ed.). Washington DC, District of Columbia, United States of America: American Association of State Highway and Transportation Officials.

AISC. (2012). *Specifications for Safety-Related Steel Structures for Nuclear Facilities*. ANSI/AISC N690-12.

AISC. (2011). *Steel Construction Handbook* (14th ed.). Chicago, Illinoise, United States of America: American Institure of Construction.

ASTM (2013) *ASTM A572-13 Standard Specification for High-Strength Low-Alloy Columbium-Vanadium Structural Steel*, ASTM International, West Conshohocken, PA

ASTM (2012) *ASTM A36-12 Standard Specification for Carbon Structural Steel*, ASTM International, West Conshohocken, PA

Brockenbrough, R. (2003). *AISC Rehabilitation and Retrofit Guide.* Pittsburgh, PA, the United States: American Institute of Steel Construction.

Budkowska, B., & Szymczak, C. (1996). Partially Embedded Piles Subjected to Critical Buckling Load - Sensitivity Analysis. *Computers & Structures , 61,* 193-196.

Culmo, M. (2009). *Connection Details for Prefabricated Bridge Elements and Systems* . McLean, Virginia, United States of America: U.S. Department of Transportation Fedral Highway Administration.

Das, B. (2010). *Principles of Foundation Engineering* (7th Edition ed.). Cengage Learning.

Davisson, M.T., Manuel, F.S. and Armstrong, R.M. (1983) Allowable Stresses in Piles, *FHWA/RD-83/059*, Federal Highway Administration, Washington DC.

Fatahi, B., Basack, S., Ryan, P., Zhou, W.-H., & Khabbaz, H. (2014). Performance of Laterally Loaded Piles Considering Soil and Interface Parameters. *Geomechanics and Engineering , 7*, 495-524.

FHWA (1998) Driven 1.0: A Microsoft Windows-Based Program for Determining Ultimate Vertical Static Pile Capacity, *FHWA-SA-98-074*

Forscht, C. (2012). *Pile Hammer Analysis Evaluation.* Pennsylvania Department of Transportation.

Goble, G.G., Rausche, F. and Likins, G.E. (1980) Driving: A State-of-the-Art, *The 1st Seminar on the Wave Theory on Piles*, Stockholm, Sweden.

Hannigan, P., Goble, G., Likins, G., & Rausche, F. (April 2006). *Design and Construction of Driven Pile Foundations-Volume I.* Washington, D.C.: National Highway Institute, Fedral Highway Administration .

Hartle, R.A., Wilson, K.E., Amrhein, W.A., Zang, S.D., Bouscher, J.W. and Volle, L.E. (2003) LRFD Design Example for Steel Girder Superstructure Bridge and Commentary, *FHWA NHI-04-041*, Federal Highway Administration, Washington DC, 648 pp.

Hussein , M., Bixler, M., & Rausche, F. (2003). *Pile Driving Resistance and Load Bearing Capacity.* Orlando, Florida USA: GRL Engineers, Inc.

Kulhawy, F. H., Trautmann, C.H, Beech, J. F., O'Rourke T. D., and McGuire, W. (1983) Transmission Line Structure Foundations for Uplift-Compression Loading. *Report EL-2870*. Electric Power Research Institute, Palo Alto, CA, 23pp

Lowery , L. L. (1993). *Pile Driving Analysis by the Wave Equation.* Texas USA: A&M University.

Meyerhof, G. G. (1976) Bearing Capacity and Settlement of Pile Foundations, *ASCE Journal of the Geotechnical Engineering Division,* Vol. 102, pp. 195–228.

McCann, D., & Peraza, D. (2008, 2). *Avoiding Structural Failures During Construction.* Retrieved 9 9, 2014, from Structural Engineering Magazine: http://www.structurearchives.org/Archives/2008-2/C-LessonsLearned-Peraza-Feb08.pdf

National Highway Institute (NHI) (2001) Load and Resistance Factor Design (LRFD) for Highway Bridge Substructures, Publication *FHWA HI-98-032* (May 2001). 592 pp.

NHI-Course-No.132068. (2001, May). Load and Resistance Factor Design (LRFD) for Highway Bridge Structures. *Reference Manual and Participation Workbook* . Washington DC, District of Columbia, United States of America: U.S Department of Transportation - Fedral Highway Administration.

Nordlund , R.L. (1963) Bearing Capacity of Piles in Cohesionless Soils, *ASCE Journal of Soil Mechanics and Foundation Division*, Vol 89, pp. 1-35.

Nordlund, R.L. (1979) Point Bearing and Shaft Friction of Piles in Sand, *5th Annual Fundamentals of Deep Foundation Design*, University of Missouri-Rolla.

PennDOT. (2014). *SOL 483-14-04 Modifications to Publication 15M-Design Manual*. Part 4 Increasing Pile Design Capacity of Piles to 50 ksi. Pennsylvania Department of Transportation.

PennDOT. (2013). *SOL 483-13-12 Modifications to Publication 15M-Design Manual*. Part 4 Increasing Pile Design Capacity of Piles to 50 ksi. Pennsylvania Department of Transportation.

PennDOT. (2012). *Pub 15A Design Manual Part 4 (DM-4) Structures.* Pennsylvania Department of Transportation.

PennDOT. (1989). *Pub 15A Compilation of Pile Load Test and Wave Equation Information.* Pennsylvania Department of Transportation.

Pile Dynamics Inc. (PDI) (2010) *GRLWEAP Wave Equation Analysis of Pile Driving*, version 2010-4.

PTC. (2011). *I-95/I-276 Interchange Pile Testing Program Summary Report.* Pennsylvania Turnpike Commission.

Robinson et al. (2006). Pile Bent Design Criteria. Raleigh, North Carolina, United States of America: Department of Civil and Environmental Engineering, North Carolina State University.

Shama et al. (2002). Seismic Investigation of Steel Pile Bents: I. Evaluation of Performance. *Earthquake Spectra , 18* . New York, United States of America: Earthquake Engineering Research Institute.

Thurman, A.G. (1964) Computed Load Capacity and Movement of Friction and End-Bearing Piles Embedded in Uniform and Stratified Soil, *Ph.D. Thesis*, Carnegie Institute of Technology.

Tomlinson, M. J. (1986). *Foundation Desing and Construction*(5^{th} ed.). Essex, England: Longman Scientific and Technial.

VDOT. (2014). Pier Details. *Design Aids - Typical Details , V*(Part 2). Virginia , United States of America: Virginia Department of Transportation.

Vesic, A. (1977). *Design of Pile Foundations, NCHRP Synthesis of Highway Practices 42.* Washington DC, District of Columbia, United States of America: Transportation Research Board.

Vijayvergiya, V.N. and Focht, J.A., Jr. (1972), A New Way to Predict the Capacity of Piles in Clay" *Proceedings, 4th Annual Offshore Technology Conference*, Vol. 2, pp. 865-874.

Watral, R.S. (2013) *Review Capacity Implication for 50 ksi Piles Bearing on Weak or Soft Rock*, memo to Tom Macioce dated 23 August 2013.

Wilson, S., & Hilts, D. (1963). How to Determine Lateral Load Capacity of Piles. *Pile Foundations: Know-How* . Seattle, Washington, United States of America: Shannon & Wilson, Inc.

WSDOT. (2014). Terminal Design Manual. (S. R. Levengood, Ed.) Olympia, Washington, United States of America: Washington State Department of Transportation.

WSDOT (2005) Development of the WSDOT Pile Driving Formula and Its Calibration for Load and Resistance Factor Design (LRFD), *WA-RD 610*.